Deliverable Report D1.41

Innovative measurements and

Sensors for control

Agreement n.:	308974
Duration	November 2012 – October 2017
Co-ordinator:	DTU Wind

The research leading to these results has received funding from the European Community's Seventh Framework Programme FP7-ENERGY-2012-1-2STAGE under grant agreement No. 308974 (INNWIND.EU)

Document information

Document Name:	D1.41Innovative Sensors for Control
Document Number:	Deliverable D 1.41
Author:	Troels Friis Pedersen, Torben Mikkelsen, Mikael Sjoholm, Nikolas Angelou, Karen Enevoldsen, Anand Natarajan – DTU Wind Energy Ervin Bossanyi – DNV GL David Schlipf – Univ. of Stuttgart
Document Type	Report
Dissemination level	PU
Review:	Anand Natarajan
Date:	Aug 30, 2015
WP:	1
Task:	4
Approval:	Approved by Project Coordinator

Table of Contents

1.0 Overview of State of the art in sensors used in wind turbine control

This introduction considers only those sensors used as key inputs to the closed loop control of pitch angles and generator reaction torque, which regulate the normal wind turbine power production and operational loading. (There is of course a vast array of other sensors feeding into the controller – everything from grid voltage and frequency, temperatures of various subsystems, motor and pump speeds, limit switches and oil level indicators to operator switches and emergency stop buttons.)

Only variable speed pitch regulated turbines are considered. The key sensor for the closed loop control is the generator speed, since above-rated pitch control is used to regulate this speed to prevent excess loading, and below-rated control adjusts this speed to maximize aerodynamic energy capture from the rotor. The wind speed sensor is normally used only to inform the supervisory controller, for example to decide whether the wind speed is high enough to initiate a start-up, or to yaw the turbine into wind. When the turbine is operating, the turbine rotor is actually a much more appropriate anemometer since it effectively measures over the whole rotor disk, while the anemometer measure a very local wind speed which is not only in the rotor shadow but also highly disturbed by flow around the nacelle and moving blade roots. Even to initiate a shutdown, using the blade pitch angle as a proxy for wind speed may result in more optimal shut-down decisions. In fact, with knowledge of the blade pitch angles together with rotational speed and acceleration, a wind turbine controller can estimate the rotor-average wind speed very effectively.

The wind vane suffers from the same disadvantages as the anemometer due to its position and small size, but is used despite this for the very important function of controlling nacelle yaw, to minimize yaw misalignment as the wind direction changes. Estimation of rotor-average yaw misalignment from other measurements, such as blade root loads for example, may be possible, but it is not straightforward to do this to sufficient accuracy in the face of other wind flow in-homogeneities. However, yaw control has to be slow to avoid overloading yaw actuators and to avoid high gyroscopic rotor loads, so the humble wind vane can actually be used very effectively for yaw control if the signal is heavily filtered, and the zero offset is well calibrated, this calibration being a function of turbine operating point because the flow direction can be significantly affected by rotor speed and blade pitch angle. Other yaw misalignment sensors such as rotating spinner-mounted anemometers and LiDARs may be able to perform significantly better in principle, but are only worthwhile if the additional cost can be justified.

Beyond the basic need to regulate rotor speed, and hence power output, the turbine controller has an important role in managing turbine loading, especially through changing pitch angles dynamically to control thrust-related loads, and adjusting generator torque to damp out torsional vibrations. The generator speed signal, which generally has high resolution and a fast sampling rate, is used effectively for the latter task, although further

improvement can be obtained if suitable measurements are available of shaft torque or in-plane blade root loads, or if rotational speed of the hub or low speed shaft is measured to sufficient accuracy to allow the twist velocity to be calculated.

The control of thrust-related loads using blade pitch is the subject of many different control enhancements, usually requiring additional sensors.

Most turbines would already have nacelle-mounted accelerometers, for example to initiate a shutdown in the event of severe structural failure. Accelerometers are relatively cheap and robust, and as long as the bandwidth is sufficient to detect the first tower mode frequency, the fore-aft component of the measured nacelle acceleration can be used to good effect in damping out fore-aft tower vibration, leading to significant reductions in tower fatigue or, in the case of floating turbines, to stabilize fore-aft pitching motion of the whole turbine. Potentially, the side-side component of acceleration can also be used to damp side-side tower vibration by modifying the generator torque, or by modifying individual pitch angles as a function of blade azimuth to modify lateral rotor thrust. This may be more important offshore, where wind/wave misalignment can cause more significant lateral vibration.

Individual blade pitch control (IPC) can be used to control asymmetric out of plane rotor loads, leading to significant fatigue load reduction, especially the blade out of plane loads and the yawing and nodding moments affecting the hub, shaft, yaw bearing and tower top, as well as support structure torsional loads. For input, the most common arrangement uses strain sensors to measure blade root bending moments. Conventional resistance-based strain gauges are not considered sufficiently reliable, being difficult to bond securely and liable to calibration drift, so fibre-optic sensors are generally preferred despite the higher cost. These can be bonded to the blade root surface, or sensor fibres can be embedded in the glass fibre layup when the blade is constructed. Temperature compensation is usually achieved by including an unstrained sensor. It is important to calibrate the sensor at turbine commissioning, which is usually achieved using the blade self-weight. Other alternatives such as laser-based deflection measurements of the blade tips have been suggested. Blade tip accelerometers are a possibility, but they do not measure the DC component and would be inaccessible for replacement in case of failure. It is also possible to measure the nodding and yawing moments directly, by measuring shaft bending strain, hub deflection, or tower top bending and torsional moments. The latter has the advantage that load cells can be bonded reliably to the steel tower surface, avoiding expensive fibre-optics, and the sensors are not on the rotating part of the structure. Blade root moments can also be inferred from these measurements. The sensors should not be too close to the yaw bearing attachment otherwise the load paths can be complex. Bending moment sensors can be calibrated using the gravity moment of the nacelle and rotor, but yawing moment calibration is more complicated.

Nacelle- or hub-mounted LiDAR can also be used to measure the incoming wind speed, which can be used to improve collective pitch control, and potentially to measure the asymmetry of the wind field as an alternative input for IPC. Lidar-assisted individual pitch control can be done in the rotating frame using the preview of the blade effective wind speeds or in the non-rotating frame using the preview of the linear horizontal and vertical wind shears. Initial lidar-assisted individual pitch has been presented in [20], where the

estimation of the wind shears in a Disturbance Accommodating Controller (DAC) has been replaced by lidar measurements. In [21] H_∞ in the rotating and non-rotating frame have been designed. In [22] feedforward controllers in the rotating and non-rotating frame have been compared, showing showed similar performance in load alleviation, but the feedforward in the non-rotating frame was more simpler to design and more tunable, making it better for real world applications. However, the benefit of lidar-assisted individual pitch control over feedback only in general is less significant compared to the collective pitch feedforward controller as pointed out in [16].

There is much interest in 'smart rotor' controls, where flaps, tabs, air jets or other aerodynamic control devices can be placed at one or more positions along the blades, to achieve a finer control of loading along the blade. This requires some additional sensors to provide information about conditions along the length of each blade. This could take the form of strain sensors distributed along the blade: fibre-optic sensors could be particularly useful because a number of sensors can be built into a single fibre, which can be included in the glass fibre layup during blade construction. Other possibilities include aerodynamic measurements such as pressure taps in the upper and lower blade surfaces. Leading edge Pitot tubes, or conceivably LiDAR-based sensors have also been proposed for measuring the local inflow, although it is important not to create excess drag with any protruding elements.

An initial study combining a collective pitch feedback controller with a wind-preview-based feedforward controller has been presented in [1]. The baseline feedforward controller is designed to cancel out in the case of perfect wind preview the effect from the rotor effective wind speed to the aerodynamic torque over the entire full load region using the static nonlinear pitch curve. This controller achieved significant load reduction on top of a sophisticated state-of-the-art feedback controller from the European Upwind project when retuning the feedback controller gains and using simulated lidar measurements [2]. Scanning the wind field of an aeroelastic simulation is important for a more realistic evaluation, since a lidar system is not able to measure a three-dimensional wind vector, but is limited to the scalar line-of-sight wind speed. In [3] wind evolution has been added additionally to aeroelastic simulations. A wind evolution model based on LES simulations and from measurements can be found in [4] and [5], respectively. Initial field testing on research turbines ([6][7][8]) and commercial turbines [9] shows, that improved rotor-speed regulation and load reduction is feasible, if the lidar data are processed carefully. Due to the limitations of lidar-measurements and wind evolution, the estimate of the rotor effective wind speed provided by a lidar system needs to be filtered cancel out all uncorrelated frequencies to avoid harmful and unnecessary pitch action. This correlation can be estimated from data or calculated from frequency-based methods [10][11]. A linear filter can be fitted to the transfer function between the lidar estimate and the rotor-effective wind speed [7] or an optimal Wiener filter can be used [12]. In [13] a linear H_2 approach has been proposed that includes the correlation directly in the control design. Additional to the filtering, the timing is crucial. Usually Taylor's Frozen Turbulence Hypothesis [14] is used assuming that the measured wind travels with the mean wind speed to the rotor. Field testing showed that the wind is slightly more delayed [7]. Investigations in [15] assume that this is due to the induction zone and that an online-adjustment of the timing can significantly improve the performance. These details are covered in more detail in [*D1.42*].

The spinner anemometer is a novel device that is placed in the spinner in the front of the turbine [23]. It uses the aerodynamics of the spinner of a wind turbine for measurement of the wind conditions experienced at the centre of the rotor. It has 3 sonic measurement devices and thereby is able to obtain a 3-D wind time series at a point in front of the turbine. The accuracy of this device is of the same level as what is traditionally obtained when using sonic anemometers mounted on met masts. However since this device is mounted on the wind turbine, it allows very accurate wind measurements for mean wind speed, std. deviation of wind speed, as well as wind direction, all of which can be used by the wind turbine controller. Further since the spinner anemometer has 3 sonics, it has a fair degree of redundancy that allows continuous measurements even if one of the sonics fails.

2.0 Measurement Capabilities of LIDARS for Control Purposes

The INNWIND.EU (http://www.innwind.eu) project has the overall objectives of developing a high performance innovative design of a beyond-state-of-the-art 10-20 MW offshore wind turbine and to develop hardware demonstrators of some of the critical components. Advanced control and input to the controllers are important aspects of the project and are investigated in particular in a task called 1.4, which is about Integrated Innovative Concepts combined with Advanced Controls. The subtask called 1.41 deals with innovative measurements and sensors for control and one of the sensors investigated is the DTU-developed Spinner Lidar. This section aims at describing the Spinner Lidar functionality and to provide a survey of lidar fault cases that a supervisory controller needs to deal with.

The Spinner Lidar is a remote sensing instrument for scanning the wind inflow to- wards a wind turbine rotor when installed either in the spinner of a wind turbine hub or on top of the turbine nacelle as seen in Figure 2.1. The instrument has been developed by the WindScanner Research And Innovation Team within the Test and Measurement Section of the DTU Wind Energy Department and its design consists of a modified ZephIR continuous-wave (cw) wind lidar and a double-prism scanner head.

Figure 2.1: The SpinnerLidar installed (left) in a wind turbine spinner and (right) on top of a wind turbine nacelle.

2.1 ZephIR lidar

The ZephIR is a cw, coherent Doppler wind lidar manufactured by ZephIR LTD (UK) and has earlier been applied for spinner-based inflow measurements [24]. The modifi- cations applied to the instrument had as an objective to provide a high streaming rate of laser Doppler spectra, as well as to allow the synchronization of the data acquisition with the scanner head. An integer number (between 4000 and 500) of Doppler spectra continuously sampled can be averaged, such that the output averaged spectra for further processing are available at selectable rates between 48.828125 Hz and 390.625 Hz.

2.2 The scanner head

The scanner head consists of two optical prisms, which rotate at constant speeds, but with a fixed gear ratio between them. The deflection angle of each optical prisms is 15◦. The fixed relative speed ratio between the prisms is 13/7, which when the deflection angle of the prisms is taken into account and with a fixed focus distance, results in a scanning pattern similar to a rosette curve (see Figure 2.2). The maximum rotation speed generates a complete scan pattern in one second, but it is possible to scan with lower speeds such that a complete scan is produced in a couple of seconds.

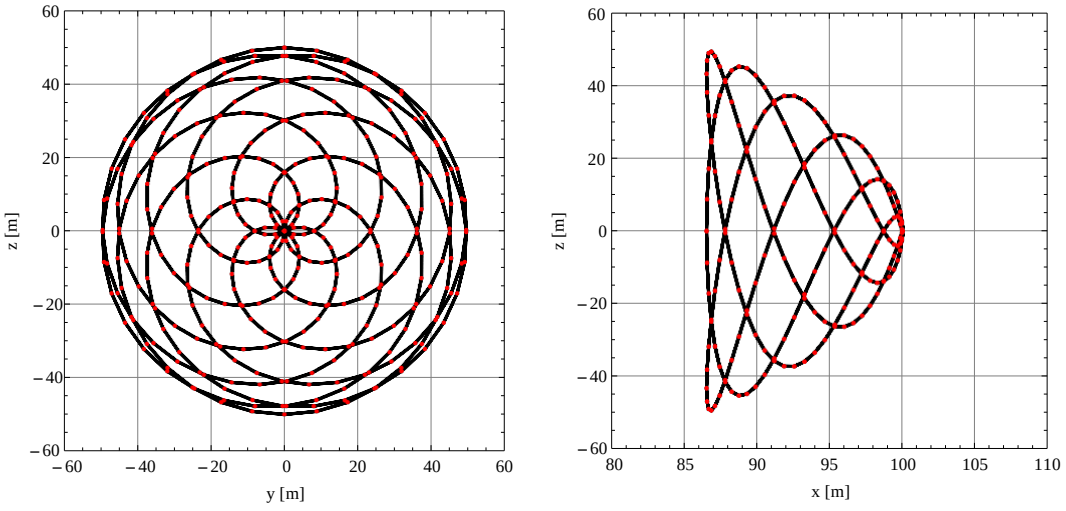

Figure 2.2: The scanning pattern performed by the Spinner Lidar seen from two perpendicular views. The pattern plotted is for a focus distance of 100 m.

2.3 Synchronization of speed and position

The Doppler spectra received by the master computer are processed for providing the estimated line-of-sight speed, the integrated spectral power and to calculate some qual- ity measures of the frequency estimation. After the completion of a full scan pattern the wind speed data is aligned with the measurement location data derived from the motion control system of the Spinner Lidar based on a common synchronization signal.

With the line-of-sight wind speeds synchronized with the measurement positions, various calculations can be done for producing the output to the turbine controller. In the current implementation, all data including the Doppler spectra are stored locally on the master computer and the measurement points closest to a pre-defined set of 200 points are selected and streamed as UDP packets to the turbine gateway computer for wind field reconstruction and calculation of appropriate input signals to the turbine controller.

2.4 Outputs to the turbine control system

The output format from the Spinner Lidar can easily be adapted to the requirements posed by the receiving turbine system. The current implementation streams data to the turbine system as UDP packets with the following content:

1. **V_{LOS}**
   The wind velocity (m/s) component along the line-of-sight measurement direc- tion.

2. **Azimuth**
   Azimuth angle (radians) of the measurement point.

3. **Elevation**
   Elevation angle (radians) of the measurement point relative to the symmetry axis of the scanner.

4. **Focus distance**
   The distance (m) along the beam to the point where the beam is focused.

5. **Q**
   A quality measure ($0 \leq Q \leq 1$) of the speed estimate. It is defined as the ra- tio between the signal power around (+/- 1 bin) the estimated frequency of the thresholded Doppler spectrum, to the total signal power in the whole thresholded Doppler spectrum.

6. **P**
   The total signal power (a.u.) in the whole thresholded Doppler spectrum.

7. **T**
   The time at which the measurement point was sampled. The format is (year, month, day, hour, minute, second, fraction of second).

2.5 Fault cases

For the development of turbine supervisory controllers a brief overview of possible fault cases is given here. The simple fault case is the case when no data are provided from the lidar due to some technical issues. For such a case the definition of availability is obvious. However, historical reports on availability relating to technical issues are of little relevance for future applications due to improvements of technology based on previous experience.

It is far more arbitrary how availability is defined for the more challenging cases, where the produced data in some sense is less accurate and less useful for turbine control than expected. Basically, the overall uncertainty relates to uncertainties in the estimation of line-of-sight wind speed and to uncertainties in the location in space of the measurements, but how various meteorological conditions influence the usefulness of the lidar-measured wind for turbine control still needs to be investigated.

2.6 Technical conditions

The simple fault case for any instrument is the case when the stream of data from the instrument ceases due to some technical issues, e.g., network instabilities, hardware or software break-downs. However, some technical issues like a lowered signal strength due to attenuating substances such as dirt or moisture on the optical elements in or on the lidar, will cause similar effects as discussed in the following sub-section.

2.61 Extreme backscattering conditions

There might be rare cases of clear atmosphere, for instance in polar regions or at high altitudes, when the backscattering from the atmosphere is so low that no line-of-sight wind speed can be estimated, i.e. nothing of the Doppler spectra survives the thresholding process. With a high enough spectral threshold, no erroneous line-of-sight speeds will be produced but a too high threshold will degrade the availability during events with low atmospheric backscattering. If the spectral threshold is too low, random noise peaks will contaminate the line-of-sight speed estimation. Thus, there is a trade-off between accuracy and availability that needs to be properly addressed.

A survey of factors such as weather obscurants (cloud/rain/fog/snow), and aerosol backscatter that affect availability of lidar systems for wind measurements has previously been compiled in a report within the UpWind project [25]. The worldwide loss of availability for a ground-based continuous-wave wind lidar was estimated to be 1% due to insufficient backscatter. Furthermore, the loss of availability due to rain was estimated to be less than 2 % by Hill [25]. However, it is stated in [25] that the availability estimates are based on incomplete information on atmospheric statistics and that the values of availability may be pessimistic. Generally, the availability estimates stated are related to the occurrence of the meteorological parameters on some

kind of world-wide average, which has low relevance at a particular site. In addition, for turbine mounted lidars the laser beam is more horizontal than in ground-based applications and thus the influence from possible rain induced bias on the vertical wind component is less.

Fog represents the other extreme of high backscattering and high attenuation of the laser beam, which at some level will set a limit for how far in front of the turbine the measurements can be obtained. However, at shorter measurement distances the signal strength is improved by the fog, although there might be a slight shift in measurement location towards the turbine during such conditions.

2.62 Spatial heterogeneity in backscattering conditions

Since a continuous-wave lidar probes the wind field component along the line-of-sight with a Lorentzian sampling function centred at the focus distance, wind speeds from all distances along the line-of-sight will contribute to the Doppler spectrum measured. In the case of spatially homogenous backscattering the contributions from the tails of the distribution along the line-of-sight are negligible. However, if the backscattering is much stronger in a distant cloud or some confined domain of fog, the Doppler spectrum will not originate from the location where the lidar was supposed to measure the wind.

Potentially, low cloud heights in combination with upward-directions of the laser beam could influence the lidar-based wind measurements. With increasing turbine sizes also clouds in other directions might appear. However, the correlations between wind measured in the large number of different directions pose a possibility to account for such effects and the continuous-wave lidar manufacturer Zephir lidar claims [26] regarding continuous-wave lidar availability under cloud cover that in their deployments so far they have seen no reason to filter any turbine-mounted data due to cloud.

2.64 Doppler returns from moving hard targets

An extreme case of the backscattering heterogeneity conditions is backscattering from moving hard targets. Potentially anything not moving with the speed of the wind, like falling rain drops, animals, vehicles, blades on neighbouring turbines or the blades on the local turbine influence the lidar measurements. Since the backscattering from hard targets typically is higher than from the ambient atmosphere, the Doppler signal strength can be utilized for filtering out such contributions in combination with the spatial wind distribution as discussed in the following subsection.

2.65 The influence of turbine blade returns

The Spinner Lidar was originally developed to be placed in the spinner of a wind turbine. However, if the scanning lidar is placed on top of the nacelle behind the blades of the turbine, the velocity component of the rotating blades along the line-of-sight

will also be measured since the lidar beam is not emanating from a location at the rotation axis of the turbine.

The signal strength provides a discrimination possibility since the signal strength is much higher from a moving hard target than from the atmosphere as mentioned above. In Figure 2.3 an example of the distribution of line-of-sight speed vs signal strength is given for data obtained during half an hour of measurements behind the rotating blades of a turbine. As can be seen in Figure 2.3, there is a challenge in finding the true demarcation between the blade speeds and the wind speeds, since there will always be some measurements that only partly are originating from the blades due to the finite sampling rate of the measurements, which however in principle can be dealt with already by the Doppler spectra velocity estimator.

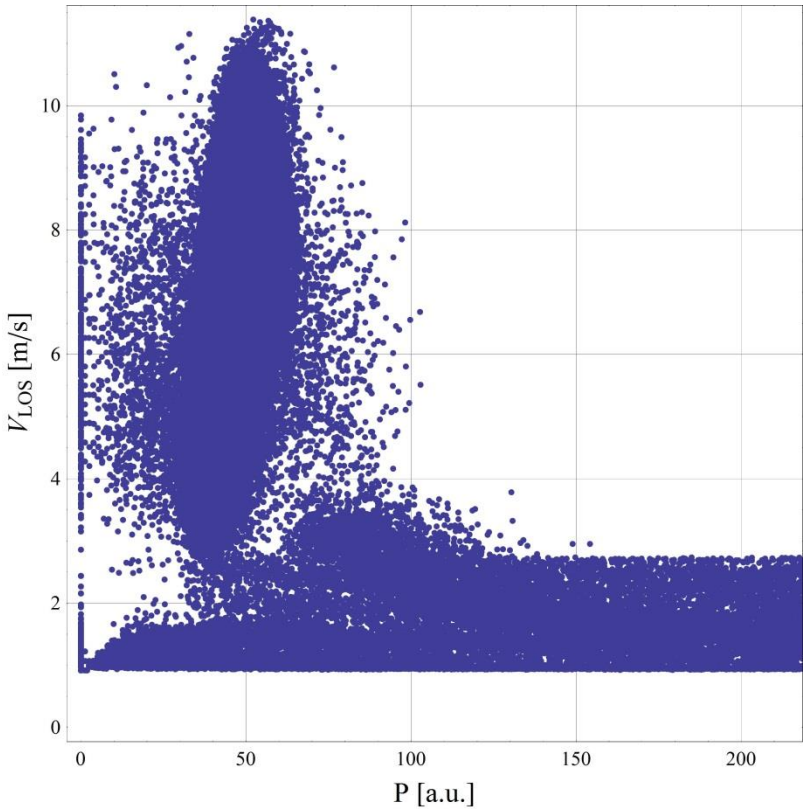

Figure 2.3: The line-of-sight speed vs the signal strength.

It can be seen in Figure 2.3 that the high signal strengths typically correspond to low speeds. This can also be seen in Figure 2.4, where the line-of-sight speed is plotted against the lateral measurement location, Sx. The v-shaped curve seen in Figure 2.4 originates from the blade returns and this upper boundary curve for pure blade returns can be estimated from the angular velocity of the turbine rotor and be used for filtering of blade returns in combination with the lower central plateau limit, which originates from the removal of the lowest Doppler range prior to the velocity estimation.

Additionally, in Figure 2.4 the central part of the scan that originates from back reflections from the outer window which corrupts the wind measurement in the

vicinity of the bore point direction can be seen. However, those measurements can easily be filtered out based on the spatial coordinates.

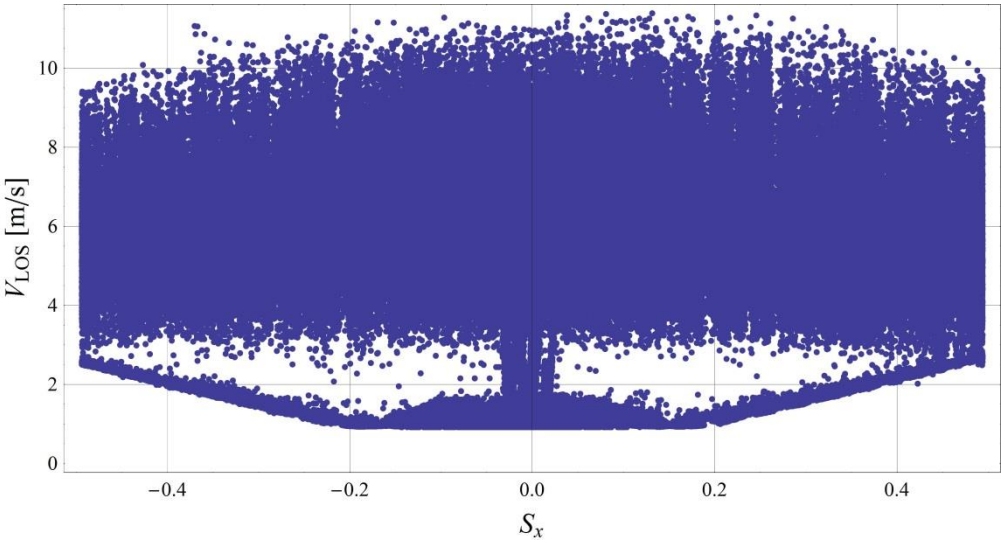

Figure 2.4: The line-of-sight speed vs the lateral scan pattern location S_x.

2.7 Lidar-Simulation

A definition of the lidar coordinate system is necessary for a lidar system simulation. The lidar system can be installed at different locations other than the origin of the inertial frame or the system can change its position and inclination, for example on the nacelle of an operating wind turbine or by rotation in the spinner. For the simulation of the lidar measurement the measurement locations, the lidar position and velocity need to be transformed in the inertial frame. All coordinates in this section are in the inertial frame. The lidar position is $[x_L\ y_L\ z_L]$.

Lidar Model for Point Measurement

A lidar system is only able to measure the component of the wind vector in the laser beam direction. Per convention, this value is positive, if the wind is directed towards the laser source. Therefore, the line-of-sight wind speed v_{los} measured at a point with coordinates $[x\ y\ z]$ can be modelled by a projection of the wind vector $[u\ v\ w]$ and the normalized vector of the laser beam, which mathematically is equivalent to the scalar product of both vectors:

$$v_{los} = x_n(u - \dot{x}_L) + y_n(v - \dot{y}_L) + z_n(w - \dot{z}_L),$$

where the normalized laser vector measuring at a distance r_L from the lidar system is

$$\begin{bmatrix} x_n \\ y_n \\ z_n \end{bmatrix} = \frac{1}{r_L}\begin{bmatrix} x_L - x \\ y_L - y \\ z_L - z \end{bmatrix}.$$

Lidar Model for Volume Measurement

Real lidar systems measure within a probe volume due to the length of the emitted pulse of pulsed lidar systems or due to the focusing of the laser beam of continuous wave lidar

systems. Additionally, the FFT involved in the detection of the frequency shift requires a certain fraction of the backscattered signal, contributing to the averaging effect.
Thus, lidar measurements are modelled more realistically considering the overall averaging effect by:

$$v_{los} = \int_{-\infty}^{\infty} (x_n(u_a - \dot{x}_L) + y_n(v_a - \dot{y}_L) + z_n(w_a - \dot{z}_L)) f_{rw}(a)\mathrm{d}a.$$

The range weighting function $f_{rw}(a)$ at the distance a to the measurement point depends on the used lidar technology (pulsed or continuous wave). The wind vector $[u_a\ v_a\ w_a]$ is an evaluation of the wind field along the laser beam at

$$\begin{bmatrix} x_a \\ y_a \\ z_a \end{bmatrix} = \begin{bmatrix} x \\ y \\ z \end{bmatrix} + a \begin{bmatrix} x_n \\ y_n \\ z_n \end{bmatrix}.$$

Lidar Data Processing for nacelle-based lidar systems
In the latest version of the Lidar library, data processing has changed substantially: Previously, scalar measurements of each measurement plane were filtered and after that shifted to compensate for the time delay as modelled by Taylors frozen turbulence hypothesis, as well as for the time delay resulting of dynamic filtering.

Now, each Lidar data sample is saved in an n-sample-long FIFO-buffer. This buffer provides the whole series of data samples, according to its previously set size. From this data, time series of Lidar measurements can be extracted and zero-phase filtering applied. This removes the necessity of compensating for phase shifts caused by dynamic filtering in the signal and also eases further processing steps like differentiation because non-causal filters can be implemented.

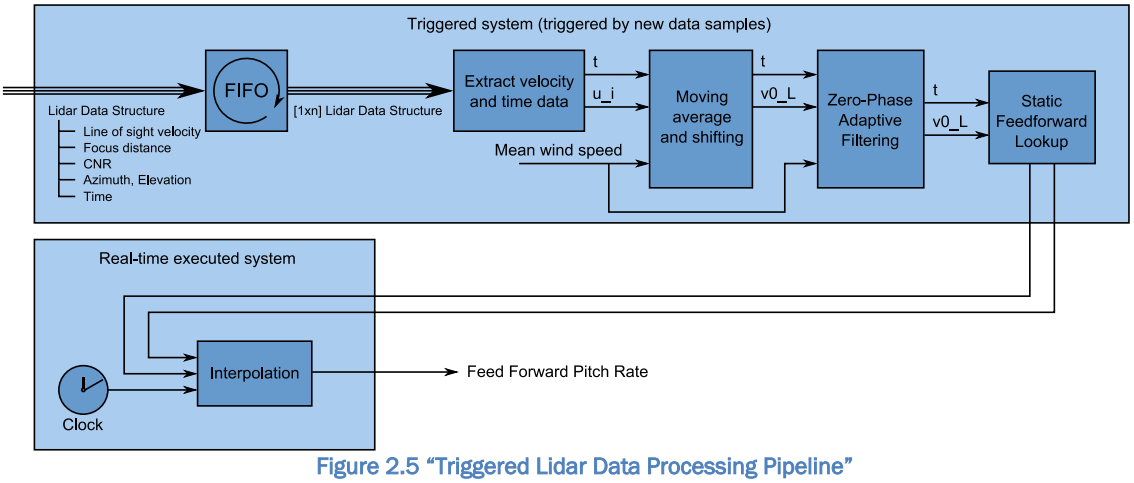

Figure 2.5 "Triggered Lidar Data Processing Pipeline"

As an additional benefit, model-predictive controllers can be fed with disturbance preview or, if an estimated rotor effective wind speed by plant data is calculated in the same way (using FIFO-buffers), an online cross correlation can be programmed, providing the time shift between the rotor plane and measurement planes as shown in Figure 2.6

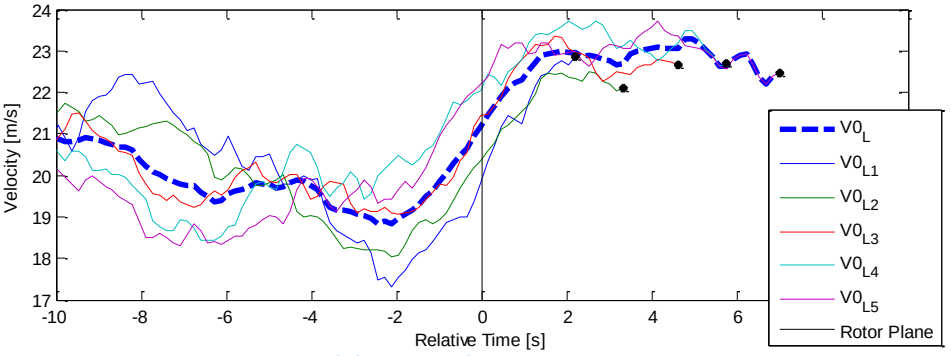

Figure 1.6 Example for online cross correlation

These alterations pave the way for an easy implementation of a variety of algorithms but come at the cost of higher memory consumption and processor load. Simulations have shown that for reasonable FIFO buffer sizes, e.g. in the range of 2-3 minutes, memory usage increases about 150kB and a modern CPU can still do all necessary operations within milliseconds.

2.8 Recommendations

It is recommended that the supervisory controller integrates an adaptive filter based on the current cross-correlation between the lidar measured wind and the wind estimated from the turbine itself similar to what was presented by Schlipf et. al in Ref. [7]. With such an approach, the feedforward input to the controller from the lidar will be cleaned from uncorrelated contributions and timely applied for optimum turbine performance. Provided that the influence from clouds, fog, etc. is relatively slowly changing, their negative influence should be possible to account for by such a correlation-based filter approach.
It is furthermore suggested that prior to the cross-correlation mentioned above, the line-of-sight wind speeds not originating from the wind field of interest are filtered out by the use of dynamically updated filters based on line-of-sight speed, signal power and measurement location in combination with yaw direction and the angular speed of the turbine rotor regarding filtering out hard target blade returns as discussed above.

The upper speed that is influenced by the local blades increase with the separation between the turbine rotation axis and the lidar scanner head and thus the separation should ideally be as low as possible. The knowledge of yaw directions in which the lidar can see other turbines in a wind farm could potentially also be utilized for more conservative filtering only in certain directions.

Regarding a numerical value of the availability of lidar-measured wind for turbine control, a proper definition of data availability in relation to the usefulness of the data for turbine control needs to be established. With such a definition in place, the relation between availability and various meteorological parameters can be experimentally investigated by field experiments. The availability at a particular site can then be esti- mated from the statistical distributions of the meteorological parameters at the site by applying the relations between those parameters and availability. However, a meteorologically

induced availability drop for turbine control is likely only relevant at locations of clear atmosphere such as for instance polar regions or at high altitudes.

3.0 Including LIDAR measurements in Wind Turbine Simulations for Load Mitigation

A wind turbine is subject to a severe wide range of loads. There are different sources of loading like aerodynamic loads, gravitational loads, inertia loads and operational loads (arising from actions of the control system e.g. breaking and pitch control) affecting the structures of the wind turbine. These loads on components of the wind turbine are sought to be reduced by the presented feedforward controller concepts. Therefore a set of simulations was put together. These kinds of simulations give a great opportunity to compare existing controller strategies und project controller performances in designed cases, which simulate all kinds of occurring sceneries. The simulations on which the following results are based on, were performed with the GH Bladed release 4.5 for the 10 MW INNWIND Turbine. This is the first release with an embedded LIDAR simulator and thus represents the opportunity to compare LIDAR based controllers on the same platform.

Over a 20 year live time of a wind turbine, structural parts of the power plant are subject to a severe level of stress. Algorithms like the rainflow cycle count are used in the analysis of fatigue loads in order to reduce a spectrum of varying stress into a set of simple stress reversals. The design fatigue load spectrum should be representative of the loading cycles experienced during power production over the full operational wind speed range, with the numbers of cycles weighted in accordance with the proportion of time spent generating at each wind speed. Having simulation results for power production over the full wind speed range weighted by their probability of occurrence over the intended lifetime (rainflow cycle count algorithm) one can condense all the stress in one component to one equivalent load, the Damage Equivalent Load (DEL). Since the fatigue load considers stress on the wind turbine components for its life time in normal operation, the DEL is a very useful reference to compare and analyse LIDAR based control concepts. Lidar based control algorithms may benefit more towards fatigue load reduction than extreme loads and therefore the key performance indicator that is to be investigated to see the effect of the LIDARs on loads reduction is the reduced variation in loads or the reduced DEL.

For lidar systems used for lidar-assisted collective pitch or generator torque control it is crucial to provide a signal of the rotor effective wind, which is sufficiently correlated to the wind speed affecting the turbine to improve the control performance. However, there are several interacting effects which determine how well the wind speed is predicted. The approach presented in **Error! Reference source not found.** models the correlation between lidar systems and wind turbines

using Kaimal wind spectra. The derived model accounts for different measurement configurations and spatial and temporal averaging of the lidar system, and different rotor sizes. Wind evolution models can also be included, but is not considered here.

One of the advantages of the correlation model is that the correlation can be calculated directly with relatively low computational effort. This can be exploited to optimize the scan configuration of lidar systems. In principle, nonlinear solvers could be applied to this optimization problem to converge faster and closer to the optimum. Here, a brute force optimization is done to display the impact of all variables.

In the next section, a scan trajectory of the SWE Scanning lidar system is optimized for measuring the rotor effective wind speed from the nacelle of the DTU 10MW reference wind turbine. Then the same approach is used to find an optimal configuration for a continuous-wave lidar installed in the spinner of the DTU 10MW reference wind turbine. The optimal trajectories will then be used for the simulations described in the Deliverable D1.42.

Trajectory optimization of a pulsed, nacelle-based lidar system

An optimization problem consists typically of a cost function (what should be optimized), optimization variables (which parameter can be changed), and constraints (which conditions have to be fulfilled).

In the case of finding an optimal configuration for a lidar system, the cost function depends on the application. In this case, the lidar system should provide a signal of the rotor effective wind speed for collective pitch feedforward control, which is correlated to the rotor effective wind speed felt by the turbine in an optimal sense.

There are several possibilities, how to define the “optimal sense”. Measures in the time domain such as the mean square error or the correlation coefficient are very useful measures under simulation conditions. Those measures are also simple to determine from field testing data. However, they sum up effects over all frequencies. This is problematic, because real signals of the rotor effective wind speed estimated from turbine or lidar data often differ from simulated ones in the way that they include noise from the measurements or the lidar movements. With frequency-based measures one can focuses on the relevant frequency domain and thus avoid these effects. But frequency-based measures are unfavourably more difficult to determine.

The choice of the optimization variables depends on the flexibility of the lidar system. In the case of the SWE-scanning lidar system, a circular trajectory has been chosen due to simplicity and is parametrized by the following variables:

- Number of points on a circle n_p

- radius of the circle normalized by its distance from the rotor r
- position of the first circle x_1

The constraints in the present optimization problem can be divided into constraints of the lidar system itself and in constraints from the requirements from the applications.

The constraints for the SWE-scanning lidar system are:

- Due to mechanical constraints, the radius r has to be between 0 and 0.5 D.
- The acquisition time is chosen to 0.2 s
- The maximum distance is ca 200 m. Since the trajectory will be used for simulations, where wind evolution is not included, larger distances will be beneficial for the trajectory to minimize the cross-contamination effect from the lateral and vertical wind speed components. Thus, for this trajectory optimization the last distance is fixed to x_5=1.1 D.

The maximum coherent wavenumber can be determined for each setting of the optimization variables and a given mean wind speed.

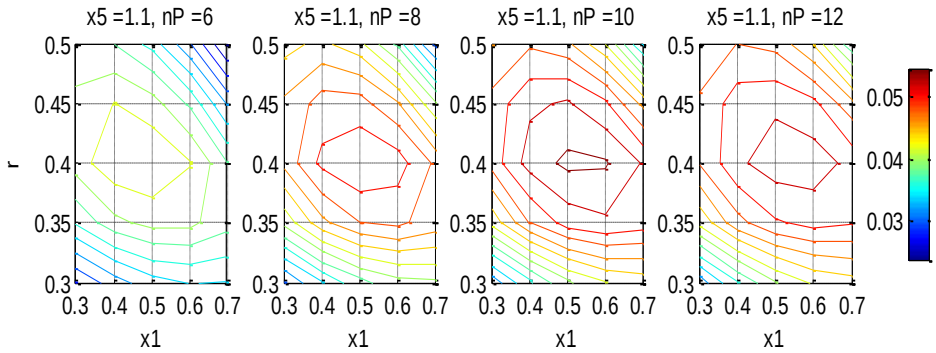

Figure 3.1: Optimization Results: Coherence bandwidth for different trajectory settings.

Using GH Bladed and based on the above algorithm for reading in the wind field, a simulation of DLC (design load cases) 1.2 at a mean wind speed $\bar{u}$ = 16m/s is run to show the capability of feed forward control. A Class "A" wind field with normal turbulence at a intensity of 17.6% (IEC Class "A") is used.

In Fig. 3.2, the baseline controller (red) is compared to the static nonlinear feedforward controller combined with the baseline controller (blue). The behavior shows that especially in the rotor speed Ω, deviations were reduced significantly. Also it can be seen that the fore-aft movements in the tower x_T are reduced with the feedforward controller. This leads to a reduction of the loads in the tower base.

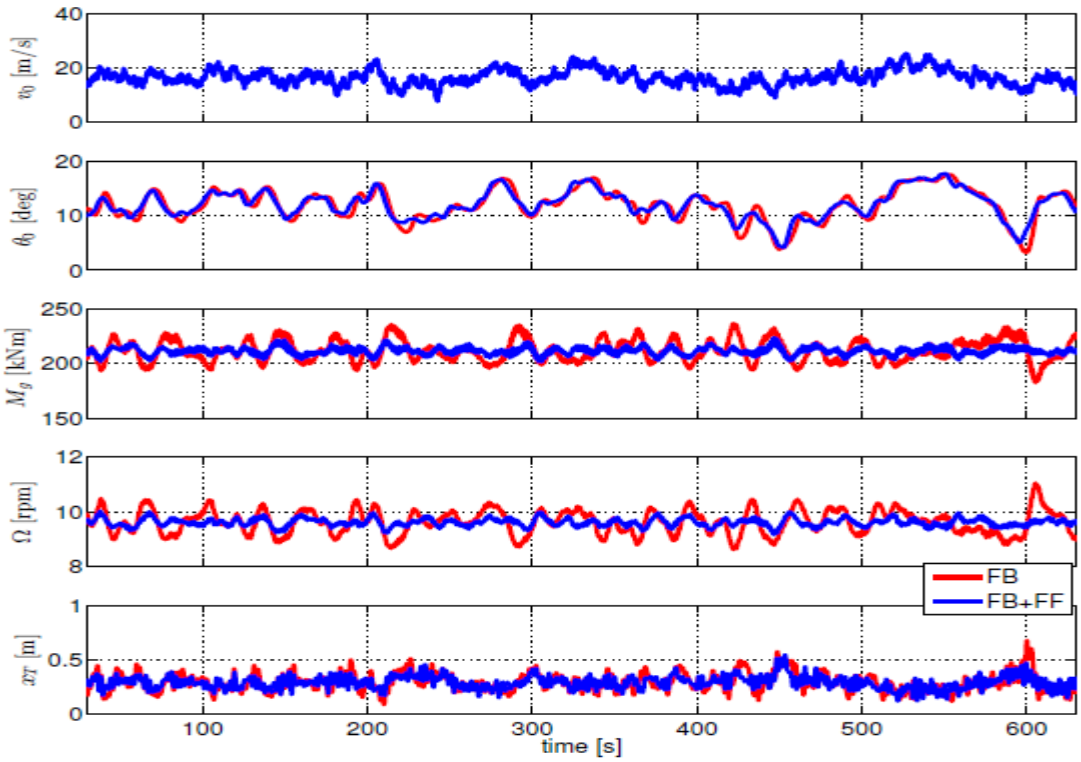

Figure 3.2: Simulation of DLC12 at a mean wind speed $\bar{u}$ = 16m/s. The baseline controller (red) is compared to the baseline + static nonlinear feedforward (blue).

Figure 3.2 describes the corresponding power spectra of the turbine states.The integral of the Power Spectral Density (PSD) is the standard deviation. This means that lower values in this graph mean lower deviations from the steady states and therefore lower values are beneficial for the lifetime of the wind turbine. The PSD of the tower base bending torque M_{yT} also shows, that the reduction is mainly to the low frequencies since the oscillations at the tower Eigen frequency (0.3Hz) is not affected. Table 3.1 shows the associated standard deviations to Figure 3.2 and the potential improvements of the feedforward controller compared to the baseline controller that is possible.

Table 3.1: Standard deviations shows the improvement of the feedforward controller compared to the baseline controller.

Standard deviations			
	$\sigma(M_{yT})$	$\sigma(\Omega)$	$\sigma(\theta)$
FB + FF	−28%	−68%	−22%

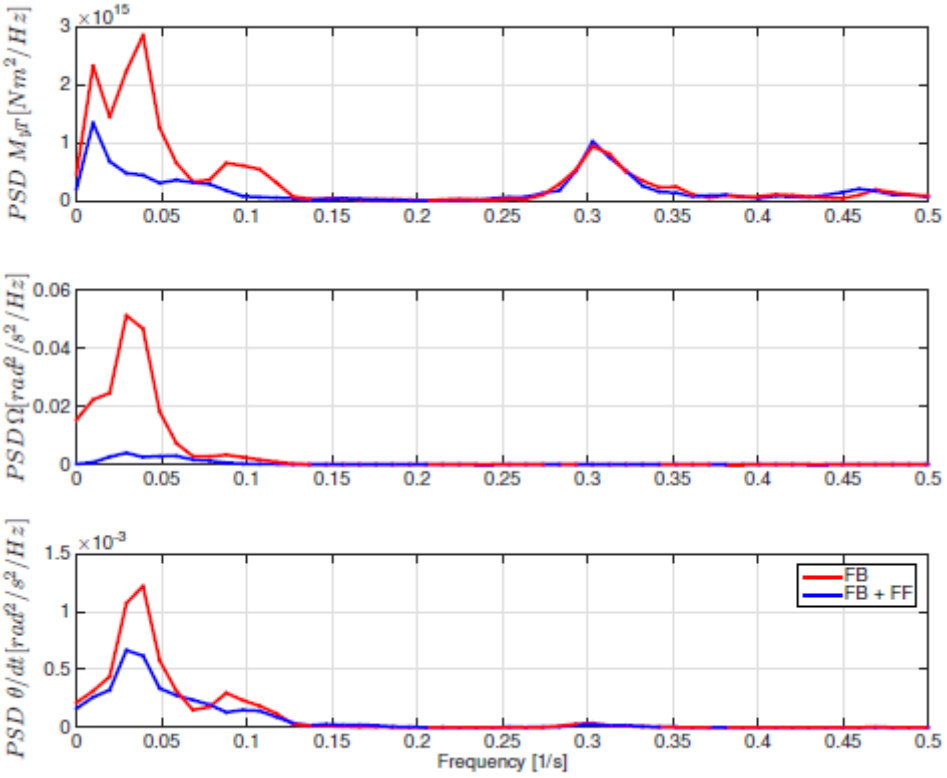

Figure 2.9: Power spectral densities of DLC 1.2.

The used of different means of LIDAR measurements in wind turbine control and the reduction in extreme and fatigue loads possible is explained in further great detail with several results in deliverable D1.42.

4.0 Spinner Anemometer Measurements and Capabilities

4.1 Measurement principle

The spinner anemometer measures the directional wind velocity in three positions on the spinner, as shown in **Error! Reference source not found.** with three sonic sensors. The spinner anemometer also has a built in rotor azimuth sensor. Each sonic wind speed sensor has a built-in accelerometer in the sensor foot which is used to determine the rotor azimuth angle of the rotor. Flow speeds around a spinner are shown in **Error! Reference source not found.**. From the stagnation point in the centre of the spinner the flow accelerates over the surface and reaches flow speeds above the free wind speed. The sonic sensors are normally positioned on the spinner where the flow speed is the same as the free wind speed.

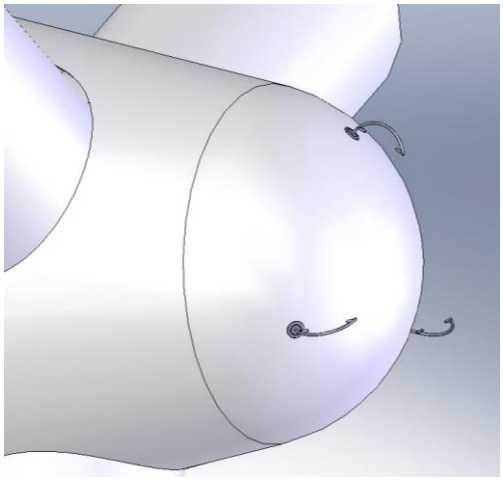

Figure 4.1 A spinner anemometer consisting of a er mounted with three sonic sensors with an erometer mounted into the foot of each sonic sensor

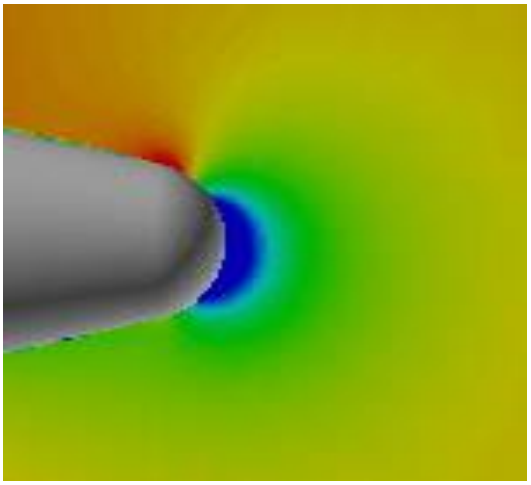

Figure 4.2 Flow speed contours around a spinner with wind from the right at a flow inclination angle of -10°, which means flow coming from below

The spinner itself may have different shapes, being semi-spherical or more pointed. The flow over different spinner shapes is also different. The assumptions in the spinner anemometer algorithm on the flow is that with an axially aligned wind the sonic sensor path flow speeds are proportional to the wind speed. At non-axial wind the sonic sensor path flow speeds are assumed to be sinusoidal over one rotation and the average flow speed over one rotation is reduced with the cosine of the angle of the wind flow to the rotor axis and the amplitude of the sinusoidal variation is increasing with the sinus to the same inflow angle. The assumptions were verified in the wind tunnel experiment [27] for a conical spinner with a semi spherical nose.

The sonic sensors measure directional wind. This means that the transversal flow speeds on the sonic sensor paths due to the rotation of the spinner are cancelled out. This also means that rotation of flow in front of the spinner due to induction by the rotor is also cancelled out.

The assumptions made for the spinner anemometer conversion algorithm is that the spinners have shapes that develop aerodynamic flow which is applicable to the conversion algorithm, and that the spinners are produced with accurate rotor symmetric geometry and that the sonic sensors are mounted perfectly correct. This is not the case. Spinners are not perfectly symmetric in geometry and they are not perfectly mounted. The sonic sensors are not mounted perfectly on the spinners, neither. But this can be compensated for. Compensation is made by making the requirement that each sonic sensor shall measure the same average flow speed over a longer time, and that the average of the three is the same. This compensation assures that the measurements during one rotation are not prone to 1P variations. Without the compensation the average measurements of the spinner anemometer over several rotations will be the same. A remarkable feature of the spinner anemometer is that angular measurements close to zero angle of attack (axial flow) can be made with very high accuracy. This is because each sonic sensor measures on either side of the flow due to the rotation, and only when the flow speeds on either side are the same, the flow is axial. This principle is also used in wind tunnels to determine flow direction. When the pressure on either side of a wedge is measured in one position, and then turned 180º, then the correct flow angle can be determined.

4.2 Conversion algorithm for three-bladed wind turbines

4.2.1 3D conversion algorithm for wind measurement

On a three bladed wind turbine three sonic sensors are mounted on the spinner in front of the gaps between the blade roots. The conversion algorithm relates the sonic sensor path flow velocities to the free wind speed and flow direction. The free wind speed is considered as the free wind speed at stand still of the rotor. This means without the influence of the rotor induction and without the drag of the spinner, blade and nacelle arrangement. The generic relation between the sonic sensor path flow velocities V_1, V_2, V_3, the free wind speed U and the inflow angle to the rotor axis α at the azimuth position of the flow stagnation point on the spinner θ is then:

$$V_1 = U(k_1 \cos\alpha - k_2 \sin\alpha \cos\theta)$$

$$V_2 = U(k_1 \cos\alpha - k_2 \sin\alpha \cos(\theta - \frac{2\pi}{3})$$

$$V_3 = U(k_1 \cos\alpha - k_2 \sin\alpha \cos(\theta - \frac{4\pi}{3})$$

These generic equations include the two spinner anemometer algorithm constants k_1 and k_2. The ratio between the two constants $k_\alpha = k_2/k_1$ is a factor that must be calibrated to measure flow angles correctly. The constant k_1 is then determined for measurement of free wind speed U.

The transformation from sonic sensor measurements to spinner anemometer parameters follows four steps, described in detail in [28]. It converts the sonic sensor path flow velocities and the rotor azimuth position φ to horizontal wind speed, yaw misalignment and flow inclination angle with the direct transformation, shown in Figure 4.3.

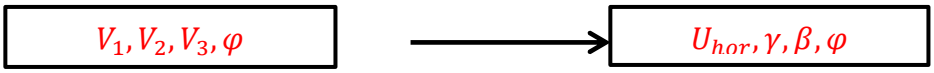

Figure 4.2 Direct transformation from sonic sensor flow velocities to spinner anemometer parameters

The first transformation step relates the sonic sensor flow velocities V_1, V_2, V_3 to the free wind speed U, the inflow angle to the rotor axis α and the azimuth position of the flow stagnation point on the spinner θ in the rotating spinner anemometer coordinate system. These parameters are directly derived from the generic equations:

$$\alpha = atan2(\frac{k_1\sqrt{3(V_1 - V_{ave})^2 + (V_2 - V_3)^2}}{\sqrt{3}k_2 V_{ave}}$$

$$U = \frac{V_{ave}}{k_1 \cos\alpha}$$

$$V_{ave} = \frac{1}{3}(V_1 + V_2 + V_3)$$

The second transformation step converts the parameters to three wind speed components $U_{x,s}, U_{y,s}, U_{z,s}$ in the non-rotating shaft coordinate system taking the rotor azimuth position φ into account. The third transformation step converts the parameters to three wind speed components U_x, U_y, U_z in a fixed nacelle coordinate system taking the shaft tilt angle δ into account. The fourth transformation step converts the parameters into the horizontal wind speed U_{hor}, yaw misalignment angle γ, flow inclination angle β and rotor azimuth position angle φ.

The inverse transformation can be made with the four transformation steps to derive the flow velocities for each sonic sensor as shown in Figure 4.4. The inverse

transformation is used when measured data with certain constants k_1, k_2, δ is to be converted to data with new constants.

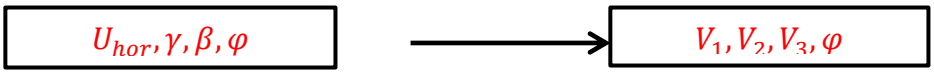

Figure 4.3 Inverse transformation from spinner anemometer parameters to sonic sensor flow velocities

The details of the transformation steps with derivation of all equations are available and best described in [28].

4.2.2 Conversion algorithm for rotor azimuth position

The rotor azimuth position angle φ is measured by three accelerometers mounted in the feet of the sonic sensors. The azimuth position of the inflow stagnation point on the spinner is defined by the angle from vertical to the azimuth position of the accelerometer in sonic sensor 1. The accelerometers within the sonic wind sensors are oriented so that they measure acceleration tangentially to the rotation, and perpendicular to the rotor shaft. In this way the centrifugal forces on the accelerometers are zero at all rotational speeds. The coordinates system and definition of parameters is described in Figure 4.4.

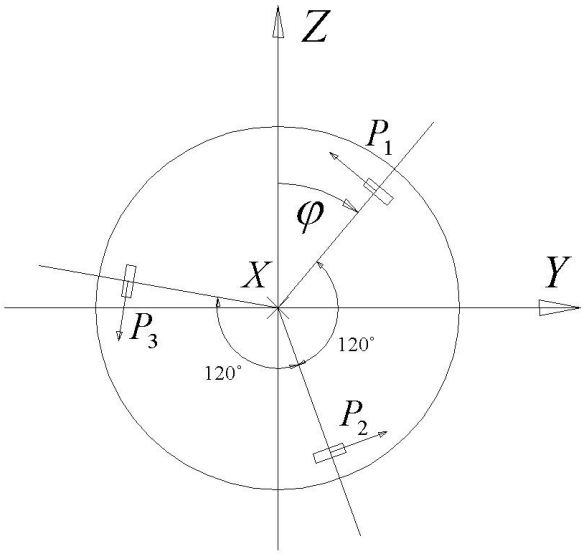

Figure 4.4 Sketch showing positioning of the three accelerometers as seen from the front of the spinner in the non-rotating shaft coordinate system. Gravity acceleration is downwards.

The three accelerometers will measure a sinusoidal signal during rotation:

$$P_1 = -G \sin \varphi + A_t$$
$$P_2 = -G \sin(\varphi + 2\pi/3) + A_t$$
$$P_3 = -G \sin(\varphi + 4\pi/3) + A_t$$

Here G is the gravity acceleration, and φ is the rotor azimuth position, as determined from the position of sonic sensor 1 relative to the vertical Z-axis. A_t is the tangential acceleration, which, in deducing the rotor position, is eliminated by mathematics when three sensors are available.

With three accelerometers the tangential acceleration A_t is averaged out in the formulas and the influence is avoided. The shaking of the spinner is not avoided, and this will influence on the measurement. The rotor position is determined from the three 1D acceleration measurements by:

$$\sin\varphi = (2P_1 - P_2 - P_3)/3G \text{ and } \cos\varphi = (P_2 - P_3)/\sqrt{3}G$$

Taking care of the quadrant of the cos and sin function, the rotor position is determined as:

$$\varphi = Atan2\frac{\sin\varphi}{\cos\varphi}$$

4.3 Redundancy in measurements

The validity of the sonic sensor and accelerometer values is tested and the result is output in a quality code Qxyz. The x value is zero when all three sonic sensors are valid, and otherwise indicating which sensors that is not valid. The y value is zero when all three accelerometers are valid and otherwise indicating which ones that is not valid. The z value indicates whether the rotor rotational speed is high enough to use an alternative conversion algorithm using only one sonic sensor with the value zero and otherwise 1.

The conversion algorithms described in the previous chapter are used when all sonic sensors and all accelerometers are giving valid values, which results in a fast sampled output of the parameters. The instrument, however, has by nature a built-in redundancy. If just one of the three sonic sensors and just one of the accelerometers give valid signals then the instrument is still able to provide output parameters.

4.3.1 1D conversion algorithm for wind measurement

The use of just one sonic sensor can still give valid output parameter signals, but the signals are averaged with a moving average 1D conversion algorithm. Redundancy of the instrument is established by use of the 1D algorithm for each sensor, and then the valid signals are averaged before output.

With the 1D algorithm only the average wind speed $U_{hor,ave}$, the average yaw angle γ_{ave} and the average flow inclination angle β_{ave} are output. The principle of

generating the average values is a complex averaging. The averaging is made through the use of a sufficiently long dataset N_{ave} that averages over several rotations, and which supports sufficiently many data for each rotor azimuth interval. The rotor azimuth position is binned into 60 bins over the rotation, each with a width of 6º. The wind speeds measured by the sonic sensor are binned with the azimuth position, and the average wind speed is determined for each rotor azimuth bin. For the bin of the actual azimuth position of the sonic sensor and for two other bins, separated by ±120º, the 3D algorithm, described earlier, is used to generate $U_{hor,i,ave}$, $\gamma_{i,ave}$ and $\beta_{i,ave}$. The calculation is made for each new sample. In the end the values from each valid sonic sensor is averaged to $U_{hor,ave}$, γ_{ave} and β_{ave}.

In order to keep computational efforts low, a number of processes are made simple on the sacrifice of storage capacity. The N_{ave} datasets (bin-index of $\theta_{i,j}$ and $V_{i,j}$) are stored in a stack that is lifted for each sample indexed j. The just sampled dataset is included in the average wind speed value of the actual rotor azimuth bin, while the dataset in the end of the stack is withdrawn from the average wind speed value of the azimuth bin for that dataset:

$$V_{i,k,ny} = \frac{V_{i,k} \cdot N_{i,k} + V_i}{N_{i,k} + 1} \quad , \quad V_{i,l,ny} = \frac{V_{i,l} \cdot N_{i,l} - V_i}{N_{i,l} - 1}$$

All bin average wind speed values and bin number of averaging data sets are stored for all rotor azimuth bins. A stack and bin array is stored for each of the three sonic wind speed sensors. A flow chart of the 1D algorithm is shown in Figure 4.6.

The output of the spinner anemometer includes both output of the 3D algorithm as well as the average of the valid sonic sensors with the 1D algorithm.

Figure 4.5 An example spinner anemometer 1D algorithm block diagram

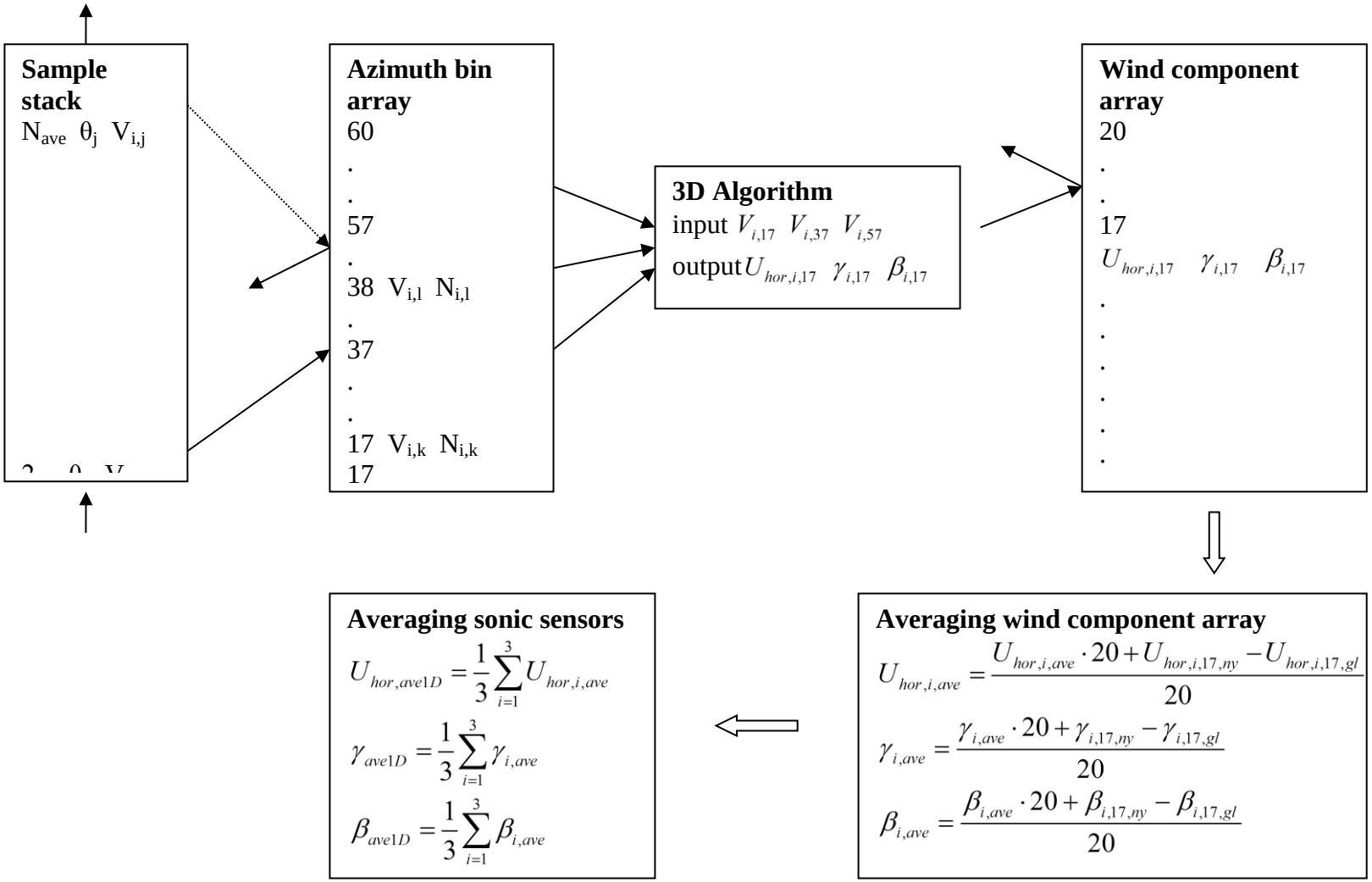

4.3.2 Conversion algorithm for rotor azimuth position with two accelerometers

An algorithm to provide output of the rotor azimuth angle is available when only two accelerometers are valid. In this case the tangential acceleration A_t is not taken into account and is neglected. An additional uncertainty during acceleration then must be considered. We then have:

$$P_1 + P_2 + P_3 = 0$$

The rotor position is determined from two accelerometers by for example the following equation, where sensor 1 and 2 are available:

$$\sin\varphi = P_1/G \text{ and } \cos\varphi = (2P_2 + P_1)/\sqrt{3}G$$

A similar equation is used for other combinations of the sensors. Taking care of the quadrant of the cos and sin function, the rotor position is determined as:

$$\varphi = Atan2\frac{\sin\varphi}{\cos\varphi}$$

An algorithm with use of only one accelerometer is also available. In this case a simple sin function is used and care is taken to what quadrant the rotor is in.

4.4 Heating of sonic sensors

The sonic sensors may accumulate ice during operation at low temperatures and under icing conditions without heating of the sensors, see Figure 4.7.

Figure 4.6: Ice build-up on non-heated spinner anemometer sonic sensor

To avoid ice to build up each sonic sensor must have a heating mechanism that heats the sonic sensor arm and each sonic sensor head at low temperatures. Testing of a heated sonic sensor in an icing tunnel at -10ºC and at 5m/s was made in [29]. Some results are shown in figure 4.8. The sonic sensor was able to provide valid signals all through the testing period of 70min.

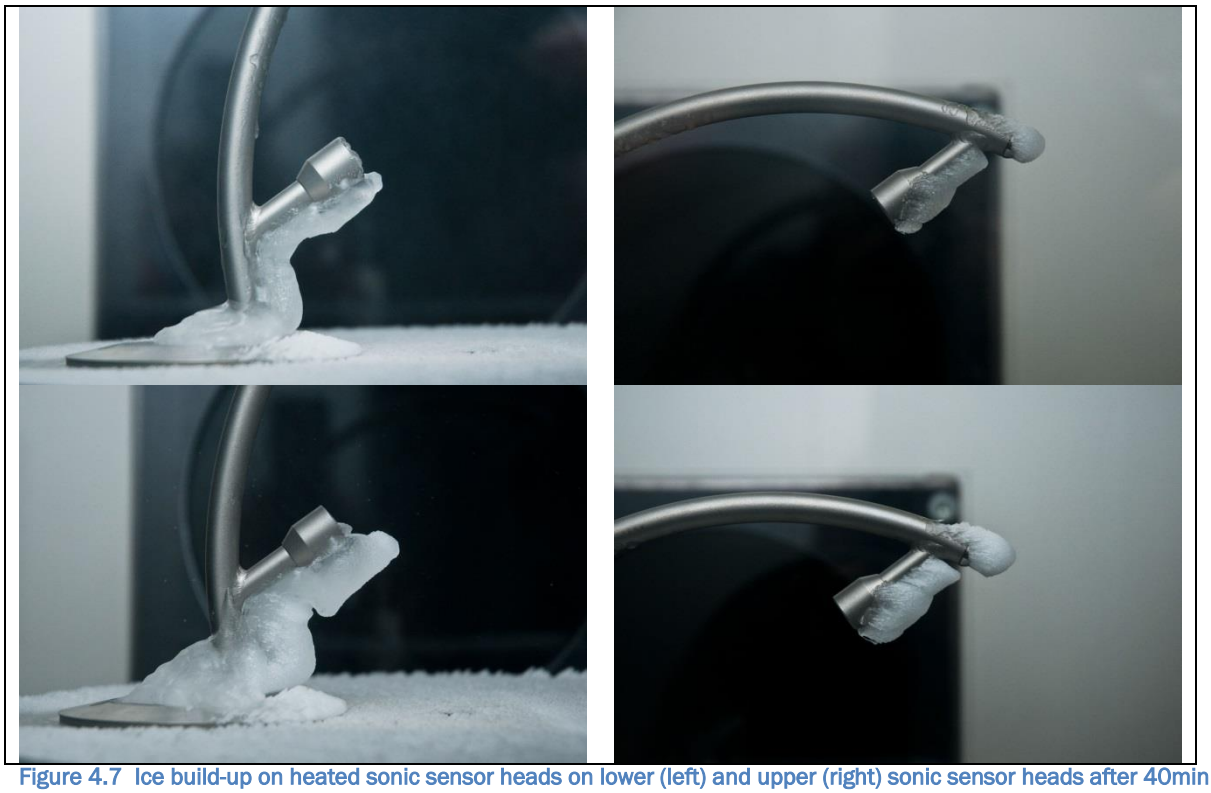

Figure 4.7 Ice build-up on heated sonic sensor heads on lower (left) and upper (right) sonic sensor heads after 40min (top) and 70min (bottom).

4.5 Instrument sensing parameters

The spinner anemometer with three sonic sensors and three accelerometers is able to output a range of parameters, partly fast scanned (10Hz) without filtering, partly averaged with a moving average algorithm (1D) but still with 10Hz output speed. The output parameters are yaw misalignment, flow inclination angle, horizontal wind speed, air temperature, rotor azimuth position and rotational speed. These parameters are all derived in the conversion algorithms.

4.6 Yaw misalignment

The spinner anemometer measures the inflow angle to the rotor, which is converted to the yaw misalignment and flow inclination angle measurements. With 10Hz sampling the yaw misalignment is an instantaneous measurement of the wind direction relative to the rotor.

Measurements of yaw misalignment have been made with spinner anemometers on quite a large number of wind turbines [30], and statistics show yaw misalignments that in many cases are quite severe [31]. An example from [31] of a yaw misalignment measurement is shown in Figure 4.9.

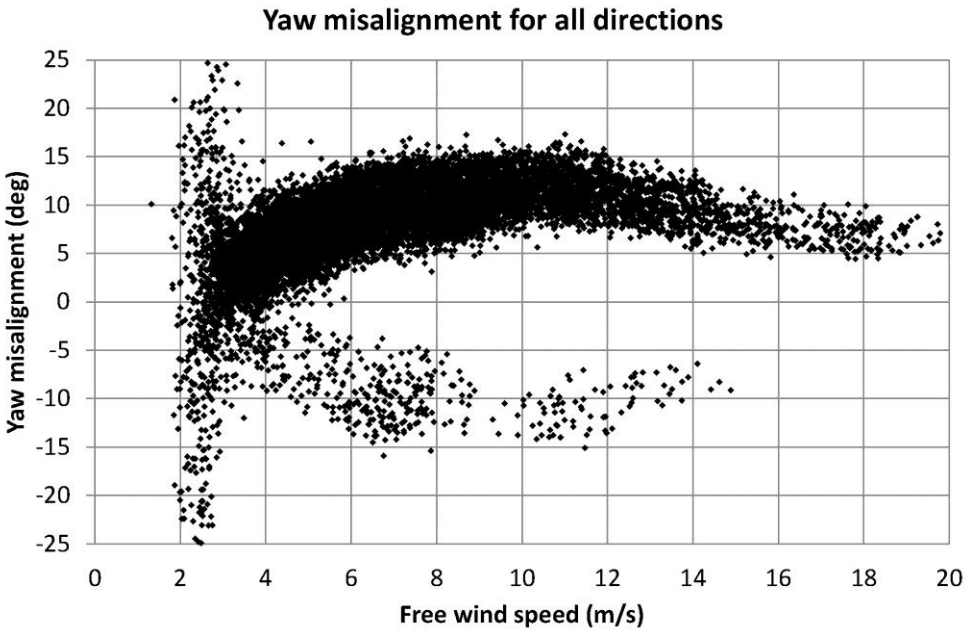

Figure4. 8 Yaw misalignment as function of wind speed with 10min averages from all wind directions including turbine wakes

The yaw misalignment here is up to more than 10° and is varying significantly with the wind speed. Some of the data show a symmetric yaw misalignment pattern. The cause of this was due to an error in

the primary nacelle 2D sonic anemometer where the secondary nacelle 2D sonic anemometer was taking over.

Yaw misalignment measurements with spinner anemometers can also be found in [27, 30, 31].

4.7 Flow inclination angle

Flow inclination angle is measured the same way as yaw misalignment. An example from [29] of a flow inclination angle measurement is shown in Figure 4.10 and 4.11. Figure 4.10 shows flow inclination measurements as function of wind speed and Figure 4.11 as function of wind direction. The measurements, which are made in very flat terrain, show that the inflow angle varies due to different causes. At high wind speeds the inflow angle is very close to zero, except for some values in the range 10-15m/s where the inflow angle is about -8º. The wind directions for these measurements were 290º to 330º, which corresponds to directions where the turbine was directly in the wake of a nearby village. The high roughness of the village shear apparently creates a downwards flow on the wind turbine of -8º. Another very evident feature is seen in figure 10 where the wake swirl behind the nearest wind turbine in the wind farm can be seen with the flow inclination variation from 15º at wind direction 190º down to -15º at wind direction 205º. Similar but smaller wake swirl from wind turbines in the wind farm further away can be seen at about 110º, 147º, 265º and 290º.

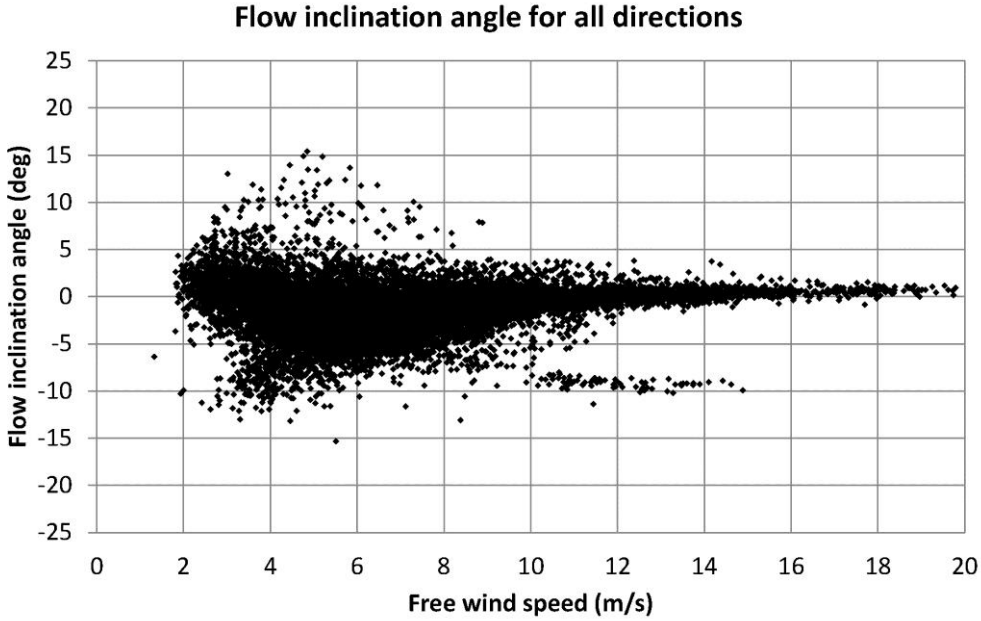

Figure 4.9 Flow inclination angle as function of wind speed (10min averages) [30]

4.8 Wind speed

The wind speed measured by a spinner anemometer is undisturbed by the nacelle and tower. The wind speed is influenced by the blade roots but this influence is integrated into the influence due to the flow over the spinner and is integrated into the calibrations. The calibration of wind speed is made so that it corresponds to the free wind speed for a stopped rotor. During operation the rotor induces wind speed in front of the rotor which slows down the wind at the spinner. The maximum slow-down is typically in the range 10-15% but varies with the wind speed. For a pitch regulated wind turbine the slow-down decreases significantly at high winds where the blades pitch out of the wind to regulate power.

Measured wind speeds of a spinner anemometer compared with a cup anemometer are shown in figure 4.17.

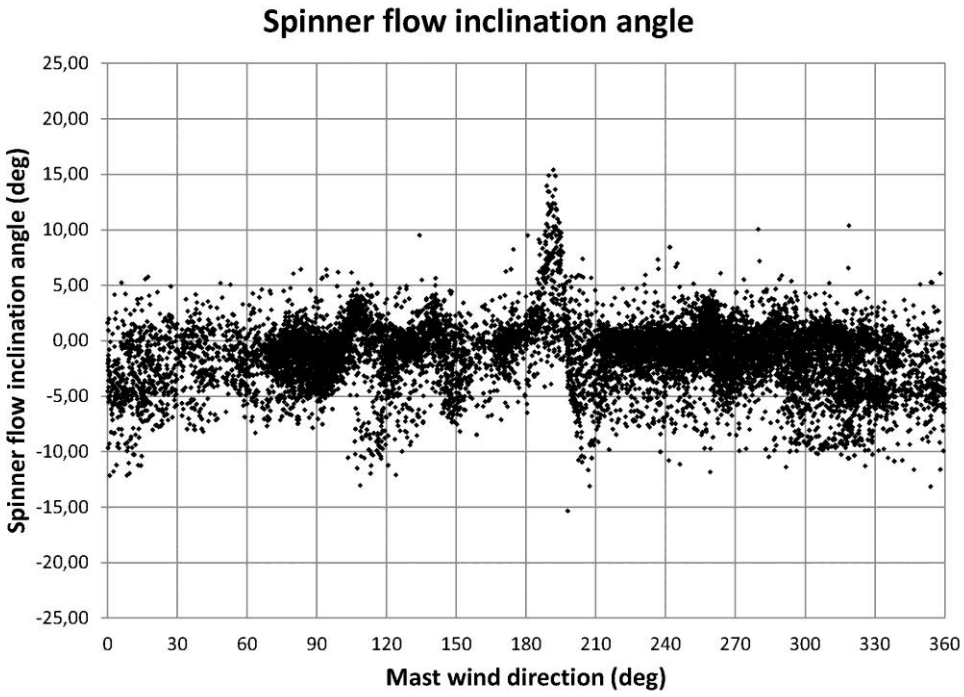

Figure 4.10 Flow inclination angle as function of wind direction (10min averages) [30]

4.9 Air temperature

The air temperature is derived from the sonic sensors. The sonic sensors measure the wind speed by sending a sound pulse from one sensor head to the other and detect the time it takes to travel over the known distance. Then another sound pulse is send from the other sensor head to the first. From the two flight times, the wind speed is calculated. The wind velocity in sensor path i is:

$$V_i = \frac{L_i K_0}{2}\left(\frac{1}{t_{i,to}} - \frac{1}{t_{i,from}}\right)$$

where L_i is the path length of sonic sensor i and K_0 is a general aerodynamic flow blockage correction factor. The sound velocity is calculated for each sensor by:

$$c_i = \sqrt{\frac{L_i}{2}\left(\frac{1}{t_{i,to}} + \frac{1}{t_{i,from}}\right) + \left(\frac{V_i}{2}\right)^2}$$

The "acoustic" temperature in Kelvin is as function of the sound velocity. For each sensor it is calculated with an approximation without taking account of the air humidity:

$$T_i = \left(\frac{c_i}{20.05 m/s}\right)^2$$

The temperature can by a spinner anemometer be determined with an accuracy of about 1K. The measurement is made on the incoming wind and is thus not influenced by radiation from the nacelle or components on the nacelle.

4.10 Rotor azimuth position

Rotor azimuth position is calculated from signals from the accelerometers mounted in the feet of the sonic sensors. They are influenced by the gravity, but also by rotor acceleration and transversal vibrations of the spinner. Rotor acceleration is cancelled out with the algorithm using three accelerometers but vibrations are still included in the signals, see example measurements in Figure 4.12. This gives some variation in the rotor azimuth position but for converting from the rotating spinner coordinate system to the fixed nacelle coordination system the influence of the variations is small.

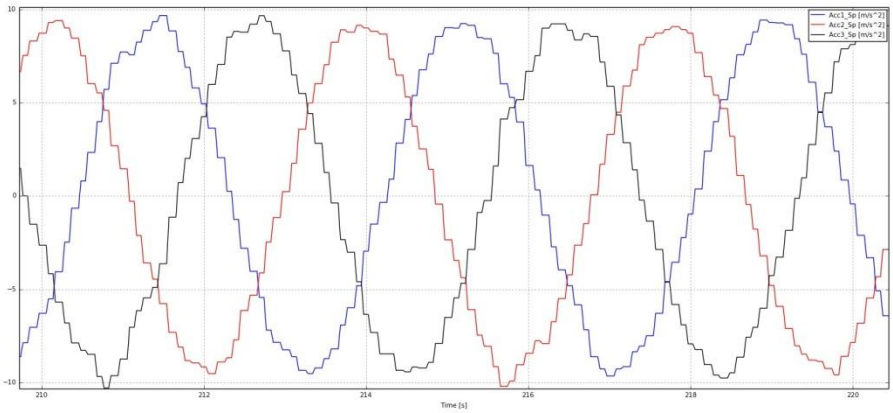

Figure 4.11 Accelerometer signals from three sonic sensors on a spinner anemometer

4.11 Rotor rotational speed

Rotor rotational speed is derived from the rotor azimuth position measurements. It is used to consider if the 1D conversion algorithm for wind measurements can be used. A comparison of measured rotational speed of a spinner anemometer signal (un-calibrated, red) with the rpm signal of the fast running shaft (blue) is shown in Figure 4.13.

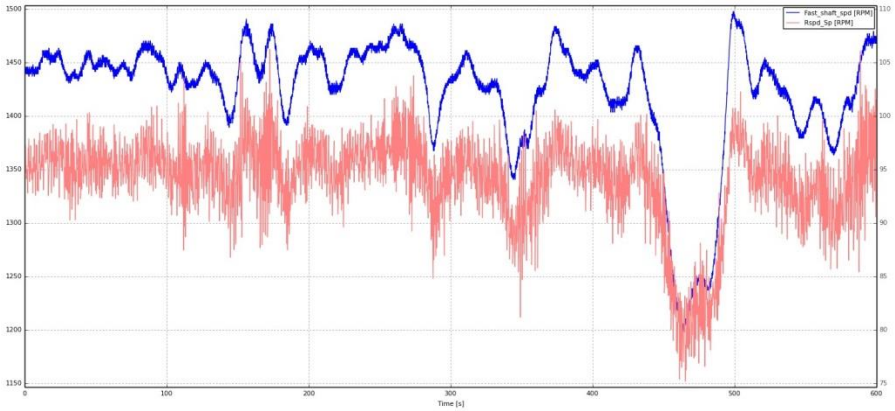

Figure 4.12 Measured rotational speed of a spinner anemometer (un-calibrated, red) compared with the rpm signal of the fast running shaft (blue).

4.12 Calibration

In this chapter the different calibration procedures are described. Calibration of the spinner anemometer is made in several steps. The calibrations are made in the order they are described here, but calibrations may be omitted dependent on the purpose of the measurements.

4.13 Zero wind calibration of sonic sensor

The manufacturer of the spinner anemometer sonic sensors and electronics box makes a zero wind calibration of individual sonic sensors in combination with the specific electronics box. A curtain is put around the sensor and the temperature inside is measured, while a calibration at zero wind speed is made by a routine in the calibration box through a communication software. With a Vernier gauge the path length between the two sensor heads is measured. The values of the path length and temperature are input to the microprocessor and are stored for the zero wind calibration and used by the basic sonic sensor algorithm. The calibration values are not changeable without doing another zero wind calibration. This procedure is a standard procedure for any type of sonic anemometer. Details of the procedure can be found in [35]. A new zero wind calibration is made if a sonic sensor is damaged on the turbine and a substitute sensor is inserted.

4.14 Wind tunnel calibration of sonic sensor

In case and accredited traceable calibration is needed for the sonic sensors it should be calibrated in an accredited wind tunnel (MEASNET tunnel). Wind tunnel calibration of a sonic sensor is very similar to calibration of a cup anemometer which is described in IEC61400-12-1 annex F [33]. A procedure has been developed for calibration of sonic sensors as part of the requirements for use of spinner anemometers for power performance verification according to the standard IEC61400-12-2 [34]. The procedure is not described in the standard, but is developed as a clarification sheet [32]. The setup is shown in Figure 4.14.

Figure 4.13 Calibration setup for wind tunnel calibration of a spinner anemometer sonic sensor [5]

The sonic sensor is mounted on a mounting plate that simulates the mounting on the spinner and keeps the flow distortion due to the sensor fitting below the plate as low as possible. The sonic sensor is mounted with the tilting angle of the sensor path (default 35.0º). The path angle has a tolerance, which must be measured at the calibration setup. Otherwise, the calibration follows the standard calibration. After the tunnel calibration the calibration line is converted to the sensor path so that the calibration in fact relates to a calibration of the sensor path at the actual measured path angle.

4.15 Internal calibration of a spinner anemometer

The general assumption for the spinner anemometer algorithm is that the spinner has a perfect rotational symmetric geometry, and that geometry of sonic sensors are perfect, and that they are mounted with perfectly the same orientation and position on the spinner. Meanwhile, the geometry of spinners is not perfect, sensors are not perfect, and mounting of sensors are not perfect. An internal calibration of the spinner anemometer has been developed which out compensates the geometric influences such that 1P variations are minimized in the output signals. The detailed procedure is described in [29] and shall not be repeated. However, the principles laid out for the calibration will be mentioned here.

Due to the mentioned imperfections the k factors may vary individually for the three sensors, though the overall k_1 and k_2 factors have been determined. To minimize the 1P influence we then have to introduce some correction factors F_{nn}, which corrects the general k factors for the local sensors. Though we have different k factors for each sensor we have to require that the average measured wind speed and flow inclination angle and the general k factors are the same over time. We want to correct each sensor so that they express the same wind speed and inflow angle over time. The internal calibration is therefore made over a certain time during normal operation, for example 30min but a longer period will improve the results. The average value of each sensor over time is an average of all

variations due to rotation and wind speed variations. If we make a "bobble sorting" of all the data from the three sensors and their average value, then we will get a span of data then we end up with sorted data on which we can make a linear regression and find the slope. The gain value or slope from this regression is a robust determination of the factors F_{nn}.

The internal calibration cannot be applied by a simple correction of the sonic sensor wind speeds. Instead a correction can be made by determining first the flow values U, α, φ from the general 3D conversion algorithm with the overall k_1 and k_2 factors. With these flow values we calculate what the corrected sensor velocities would be with the F_{nn} factor corrections. The flow velocity deviations are then determined and the deviations are applied to the measured sensor flow velocities.

The internal calibration is started during normal operation and is automatically finding the F_{nn} factors and inserting them in the box and then using them in the measurements.

4.16 Calibration for yaw misalignment measurements

The preferred method for calibration of a spinner anemometer for yaw misalignment measurements is by yawing the stopped wind turbine in and out of the wind several times in at moderate wind speeds while yaw direction and spinner anemometer output is recorded, see Figure 4.15 [28]. The measurements are plotted against each other and a linear regression is made, see Figure 4.16, where the gain is used for the determination of k_α. When k_α is inserted into the spinner anemometer box as the correct ratio between k_2 and k_1 then yaw misalignment measurements can be made in absolute values. Additionally all values of wind speed measurements are linear. This means that the non-linearity of the wind conversion algorithm no longer influences on wind speed measurements. The calibration for yaw misalignment measurements takes about half an hour to perform in the field. Before a yaw misalignment calibration an internal calibration must be made in order to make the yaw misalignment measurement independent of the rotor position during the calibration where the rotor is stopped.

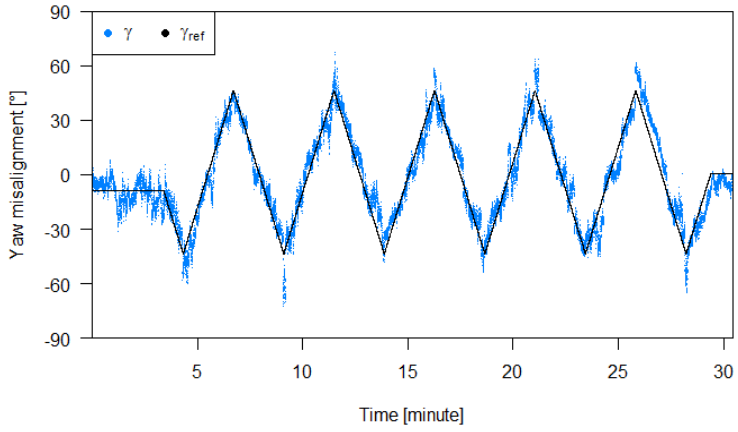

Figure 4.14 Calibrated spinner anemometer yaw misalignment measurements compared with turbine yaw direction measurements while yawing the wind turbine in and out of the wind several times [28]

4.17 Calibration for wind speed measurements

The calibration for wind speed measurements is a calibration for determination of the constant k_1 [36]. With k_α and k_1 inserted into the spinner anemometer box the spinner anemometer measures the absolute free wind speed with a stopped rotor pointing towards the wind. This also means that the spinner anemometer with k_α inserted into the spinner anemometer box can be calibrated against a reference wind speed measurement with a stopped rotor pointing towards the wind, for example using a met mast with a top mounted cup anemometer. Alternatively ground or nacelle based lidars may be used. For default settings before calibration, CFD analysis can be used for determination of k_1 and k_2 [36].

In practice, it is not feasible to stop a wind turbine for a longer time to make a wind speed calibration. In practice the calibration must take place during operation [36]. For another practical reason it is feasible to combine the calibration of k_1 with measurement of the NTF, described in [34]. By doing this the k_1 constant can be determined appropriately for very low and very high wind speeds, see Figure 4.17, and the induction part can be treated as the NTF.

Figure 4.17 shows wind speeds measured with a mast and with a spinner anemometer on an operating wind turbine where the k_1 constant was calibrated so that the measured wind speed in stopped condition and at very high wind speed corresponds to free wind speed [30]. The deviation from the blue line is due to the induction of the rotor.

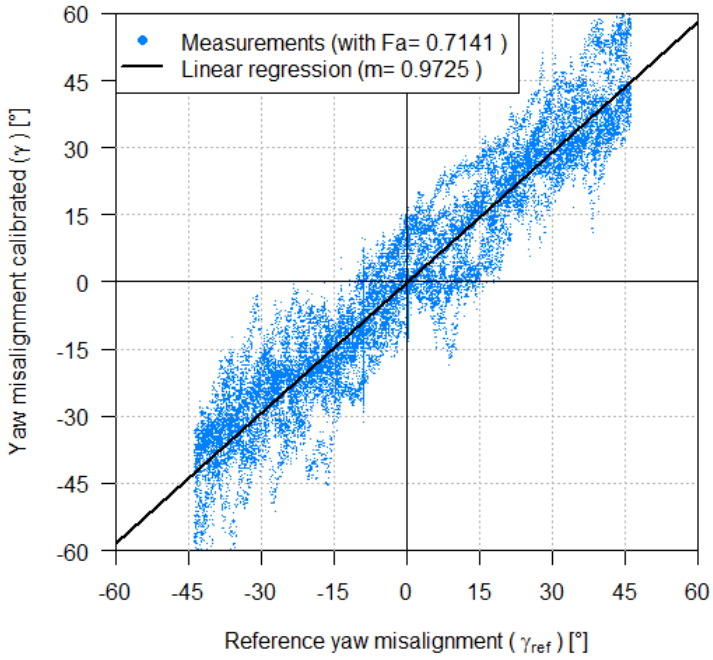

Figure 4.15 Linear regression of yaw misalignment measurements with spinner anemometer against yaw direction measurements [28]

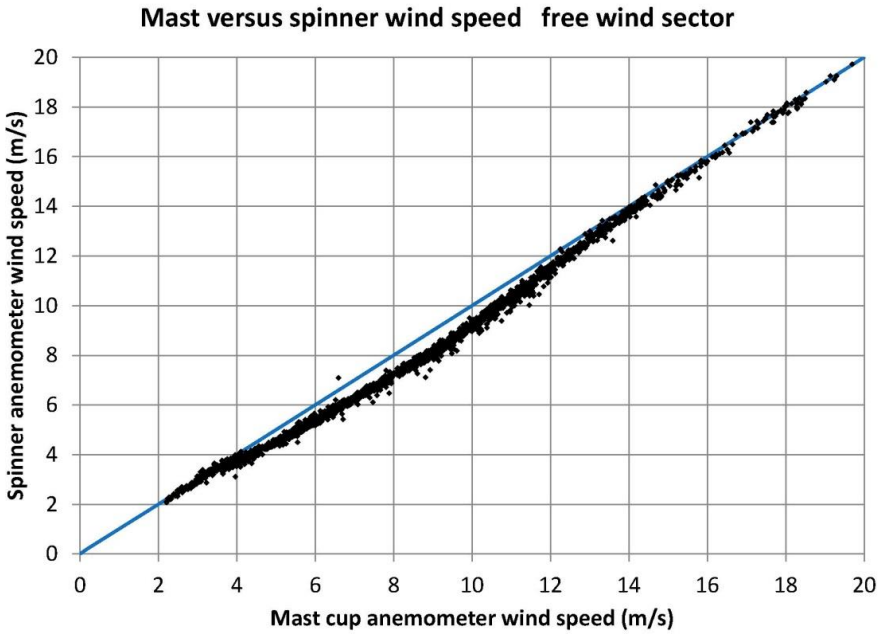

Figure 4.16 Spinner anemometer wind speed versus mast wind speed (10min averages) [30]

4.18 Calibration of nacelle transfer function

The nacelle transfer function (NTF) is the relation (a binned table of values) between the measured spinner anemometer and the free wind. As mentioned in the previous chapter the NTF can be considered to be equal to the induction in the rotor centre as the wind speed of the spinner anemometer is defined as the free wind for a stopped rotor and k_1 is determined according to this definition. The NTF could also be made directly from measurements made with a default value of k_1, but then the NTF would not represent the induction of the rotor.

The measured induction due to the rotor as a function of wind speed is shown in an example from [30] in Figure 4.18. The measured induction, which can be fitted to an induction function, can be considered as a nacelle transfer function (NTF) according to the standard IEC61400-12-2 [34]. Using the induction function or NTF one can estimate the free wind speed as shown in Figure 4.19 from [30].

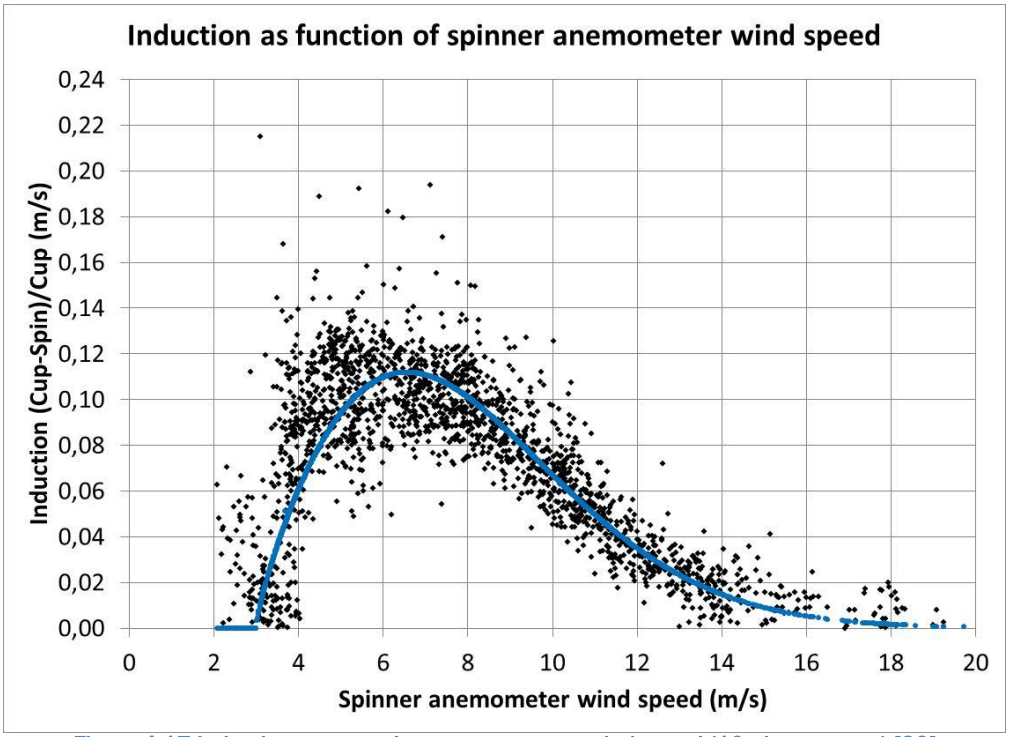

Figure 4.17 Induction versus spinner anemometer wind speed (10min averages) [30]

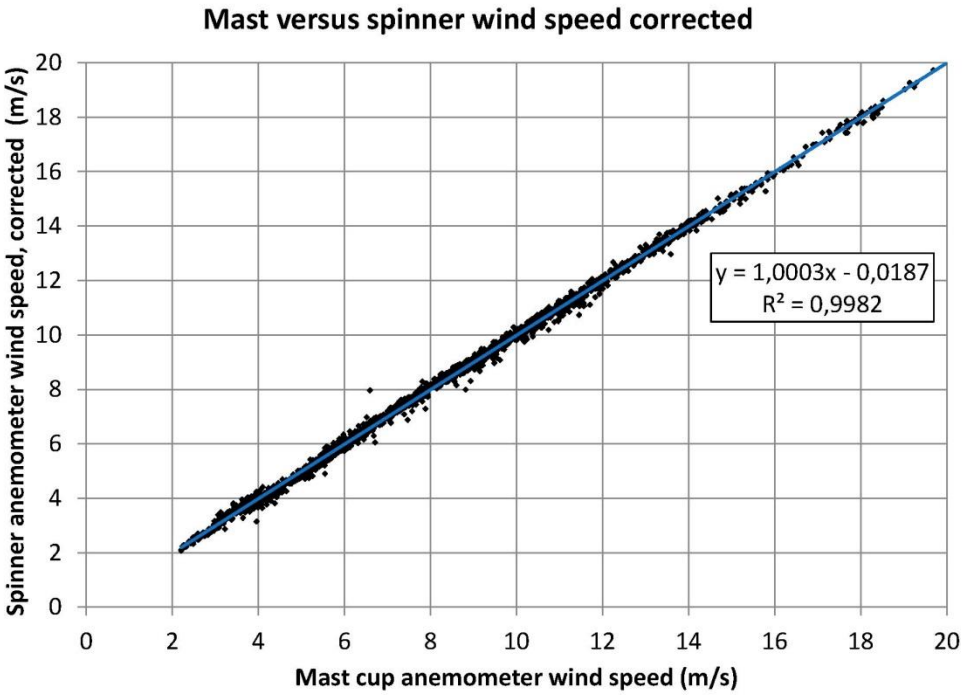

Figure 4.18 Induction versus spinner anemometer wind speed (10min averages) [30]

5. Spinner Anemometry as used for Wind turbine control

Information from the spinner anemometer may be used by the wind turbine control system in many different ways, for example active power control, correction of control settings, for measurement of power performance or loads, or for statistics or historical data logging by SCADA systems. The information may as well be used for control of the whole wind farm due to the high accuracy in wind measurements achievable. The below sub sections provide the key measurements and their means for use in wind turbine control.

5.1 Yaw misalignment

Yaw misalignment is an obvious measurement to implement into the wind turbine controller. The yaw misalignment measured by the spinner anemometer is not influenced by adjustment errors in mounting or by flow distortion due to wind turbine components. A transfer function between the measured value and the value needed for different wind speeds or other inflow conditions is not needed. The yaw misalignment is measured correctly even in wake flows with significant wake swirl with high inflow angles. This makes the yaw misalignment measurement very reliable also in complex terrain where inflow angles might vary significantly from different directions due to terrain variations.

The yaw misalignment signal may give information to the control system for yawing of the turbine, and may also give information about extreme yaw misalignments that may cause high fatigue loads or that exceed accepted limits, for example from certification requirements.

Yaw misalignment measurements may be made in relation to the standard IEC 61400-13 [33] for evaluation of load measurements.

5.2 Flow inclination angle

The flow inclination angle is a new type of measurement that has not been available on wind turbines before. The flow inclination angle measurement is made exactly the same way as the yaw misalignment measurement. The flow inclination angle is pre-set with the rotor tilt angle but it does not take the tower and shaft bending due to the thrust during operation into account. The inflow angle measurements are thus influenced by 1º-2º uncertainty at higher wind speeds dependent on the thrust.

The flow inclination angle measurements may give information to the control system about the inflow due to terrain variations, but also due to special climatic conditions, as seen with the downwards flow at high wind speed behind nearby village in Figure 4.11. Wake swirl from other turbines in the wind farm are also detectable in the inclination angle signal as seen in Figure 4.11. The inclination angle signal may also give information about extreme flow inclination angles that may cause high fatigue loads or that exceed accepted limits, for example from certification requirements.

5.3 Wind speed

The wind speed measurement directly from the spinner anemometer may be used as an alternative to nacelle anemometer wind speed measurements. The wind speed measurement is, though, without the signal distortion that nacelle anemometry has to live with. The spinner wind speed has a very high cross correlation with other parameters on the wind turbine. In Figure 5.1 the cross correlations of electrical power of a MW size wind turbine and wind speed measured with the nacelle anemometer, a mast cup anemometer, a mast sonic anemometer and the spinner anemometer are shown. The mast cup and sonic anemometers show about the same cross correlation about 0,38 at a time delay of about 40 sec while the nacelle anemometer shows a much lower cross correlation of about 0,18 with no significant time delay. The spinner anemometer show a very high cross correlation of 0.83 with no time delay.

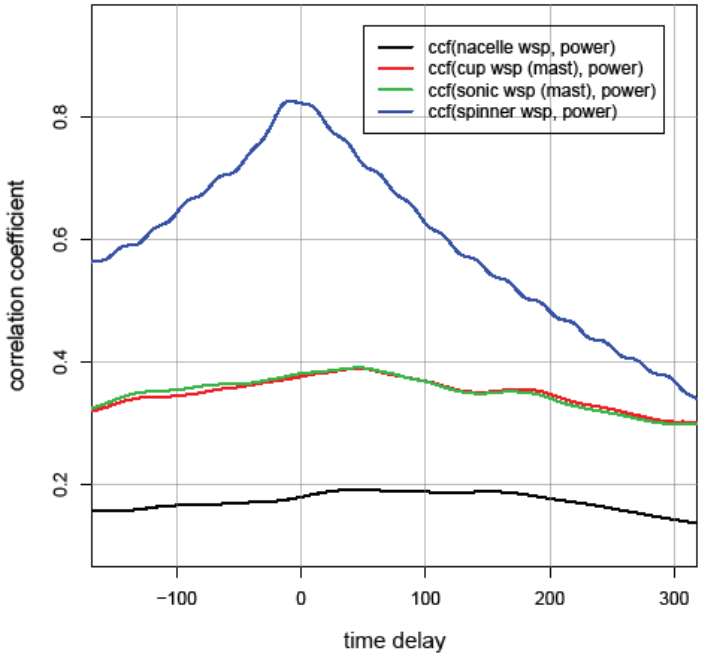

Figure 5.1 Cross correlation coefficient between electrical power and wind speed measured with nacelle anemometer, mast cup anemometer, mast sonic anemometer and spinner anemometer at 6-7m/s

This high cross correlation may be utilized to correlate parameters in the wind turbine with the wind speed or it may be used directly for information of the wind speed. In combining the measured wind speed with an NTF it will correspond to a free wind speed measurement, but in not being a distant measurement, the cross correlation to turbine parameters is high.

5.4 Turbulence

The turbulent vortices in the air are affected differently through the induction zone to the spinner, depending on the size of the vorticities. Most of the turbulent spectrum might be unaffected since the standard deviations measured from a mast and the standard deviations measured by a spinner anemometer seems to match quite well, as shown in Figure 5.2 [30]. The turbulence intensity measurement, however, is not matching the mast measurement so well, see Figure 5.3. This is because the average wind speed is influenced by the induction while the turbulent spectrum vorticities are not. When the standard deviation measured by the spinner anemometer is divided by the wind speed multiplied by the NTF function then the turbulence intensity matches quite well with the mast measurements, see Figure 5.4 [30]. This nice relationship might be coincidental for the size of turbine and turbulence structure at the site. If the turbulence spectrum consisted of larger vorticities the measured standard deviation by the spinner anemometer might have been lower. In that case a sensitivity relationship of the vorticities through the induction zone must be used.

Turbulence intensity measurements may be used to restrict operation due to high fatigue consumption in turbine components and to determine Inner Range turbulence database in performance verification.

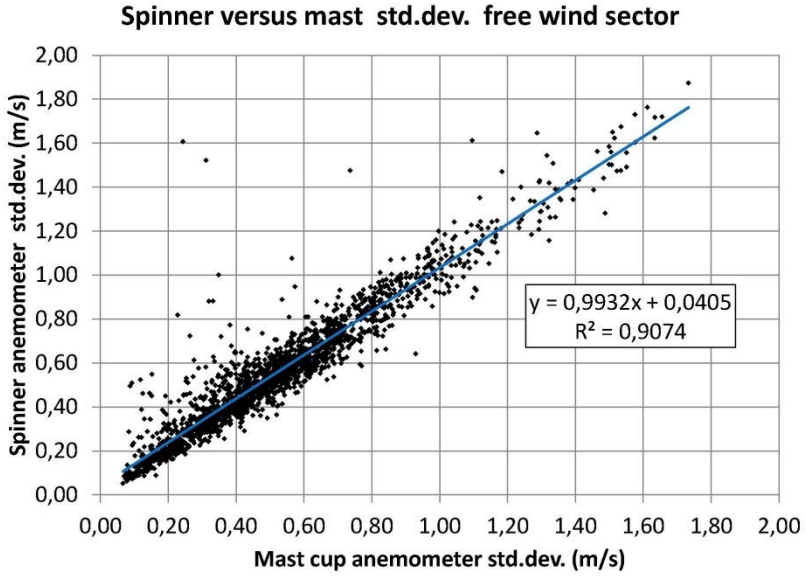

Figure 5.2 Spinner anemometer wind speed standard deviation versus mast cup wind speed standard deviation, see [30]

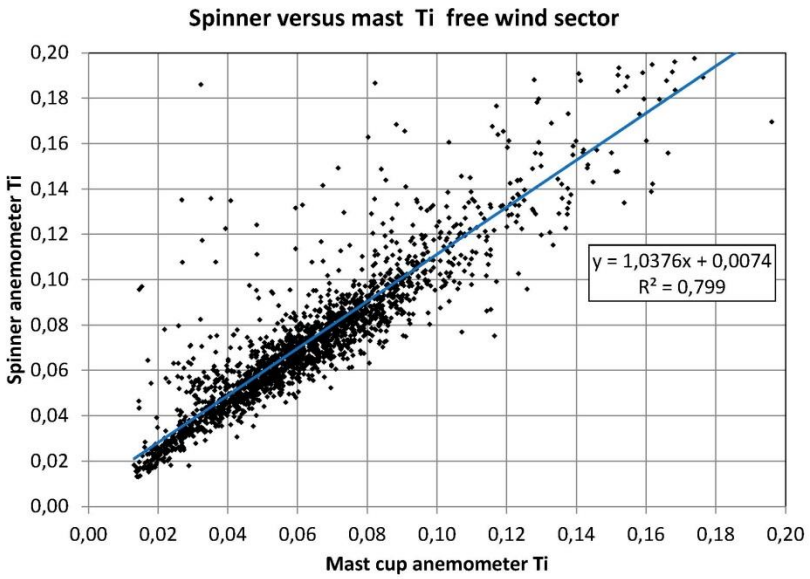

Figure 5.3 Spinner anemometer turbulence intensity without correction with NTF versus mast cup turbulence intensity, see [30]

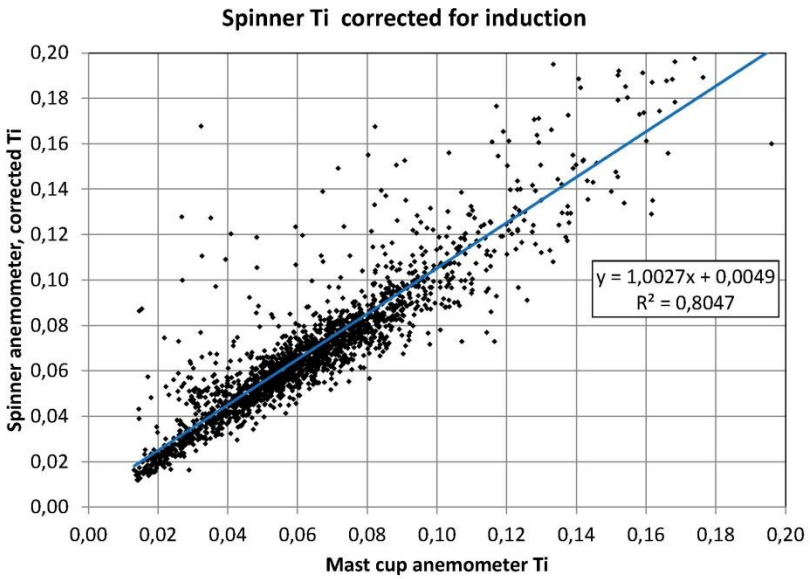

Figure 5.4 Spinner anemometer turbulence intensity with wind speed correction with NTF versus mast cup

5.5 Wind speed shear

The volume of air that actually hits the sonic sensors of a spinner anemometer is equivalent to or perhaps a little larger than the measurement volume of a standard 3D sonic anemometer. A standard 3D sonic anemometer is mainly used for turbulence and flux measurements, and so can the spinner

anemometer measure the same turbulence and flux measurements. The vertical wind speed shear, for example, may be estimated from measurement of the correlation between the components u (longitudinal) and w (vertical) [40]. The explanation for this estimation can be found in [40] as is shown in Figure 5.5. With upwards flow (w positive) and an air particle is moved from height A to height B the particle will give a negative contribution to the u component. With downwards flow (w negative) and an air particle is moved from height A to height C the particle will give a positive contribution to the u component. In both cases the uw component will be negative. The consequence is that corr(u,w) will be negative and large if the wind spear is high and negative and low if the wind shear is low.

The method is being explored at the moment and is expected to lead to a proper estimate of the shear in the centre of the rotor. The estimate cannot be based on short time measurements but will need some averaging time as the theory is based on turbulent eddies to generate the signal. The shear measurement might be used for power performance evaluation.

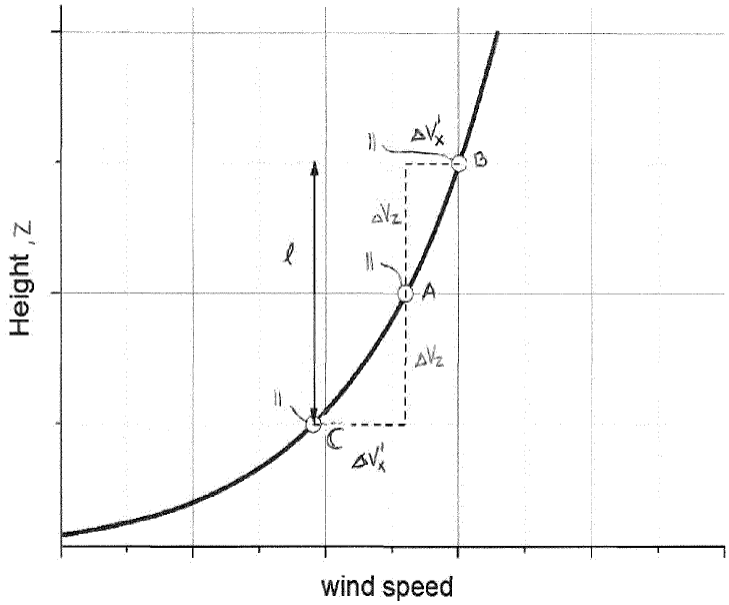

Figure 5.5 Explanation of measurement of shear [40].

5.6 Environmental conditions and wind statistics

The information that can be extracted from the spinner anemometer signals covers a range of climatic parameters. The information may be used for statistics. Wind speed statistics may be measured over periods of years and give knowledge to the actual wind resource of the wind turbine in the exact position, which can be compared to expected wind resource values.

Wind statistics may be used to verify the actual parameter variations of wind speed, turbulence, yaw misalignment, inflow angle, and temperature that the wind turbine is exposed to. Such information may be compared with values for which the wind turbine was designed for.

5.7 Power performance measurements

When all calibrations are made the spinner anemometer may be used to measure power curves according to the standard IEC61400-12-2 [34]. For this purpose, additionally signals from electrical power and air pressure must be included. An example of power performance measurements in comparison to a mast is shown in Figure 5.6 and 5.7 [29]. Figure 5.6 shows power curves measured with spinner anemometer and mast cup anemometer without use of the NTF correction and Figure 5.7 with use of the NTF correction. In this case the NTF correction function was actually derived from the same data, which of course do give a good correlation.

The aim of the standard is to transfer the measured NTF to other turbines in the same wind farm. This requires that the measurements with the spinner anemometers are performed with exactly the same measurement setup on the other turbines. This means identical spinners, identical sonic sensors and identical sonic sensor positions. In practice such ideal conditions will not exist. To a certain degree the setup conditions on the spinner can be identified by photographic techniques and variations in setup from the turbine on which the NTF was measured. Measurements to determine the NTF for transfer of the power curve to another wind turbine has been made on two wind turbines in using the same mast [37]. Methods to transfer the power curve with photographic techniques are being investigated but still not reported.

Another use of the spinner anemometer could be to keep track of power performance by comparing actual power curves measured over time with a reference power curve. Relative power curves may be made with high accuracy because the cross correlation between the wind speed and the power is very high and traceability is not a requirement [38]. Relative power curves can be made with or without the NTF correction, and they can be used to optimize power or to alert reduced performance due to wear or degradation of blades.

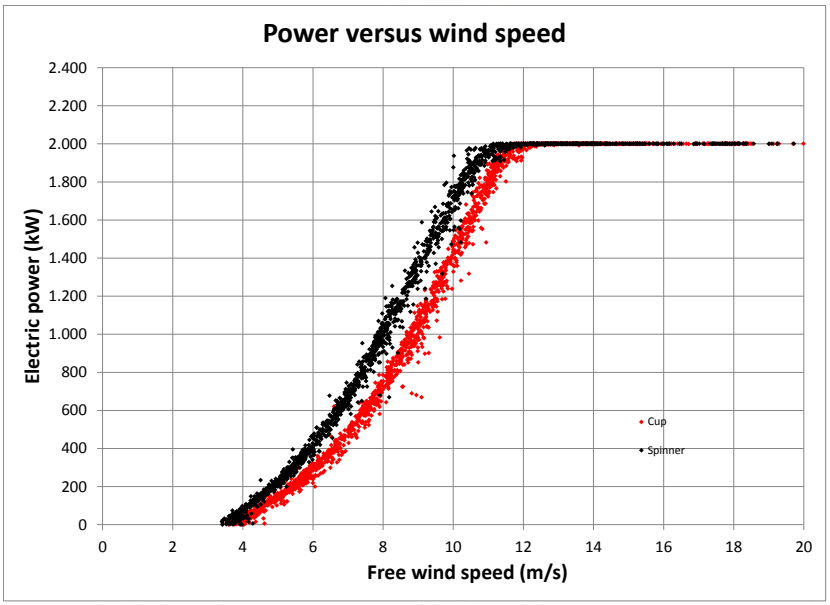

Figure 5.6 Power curves measured with the spinner anemometer (black) and the mast cup anemometer (red) without induction correction

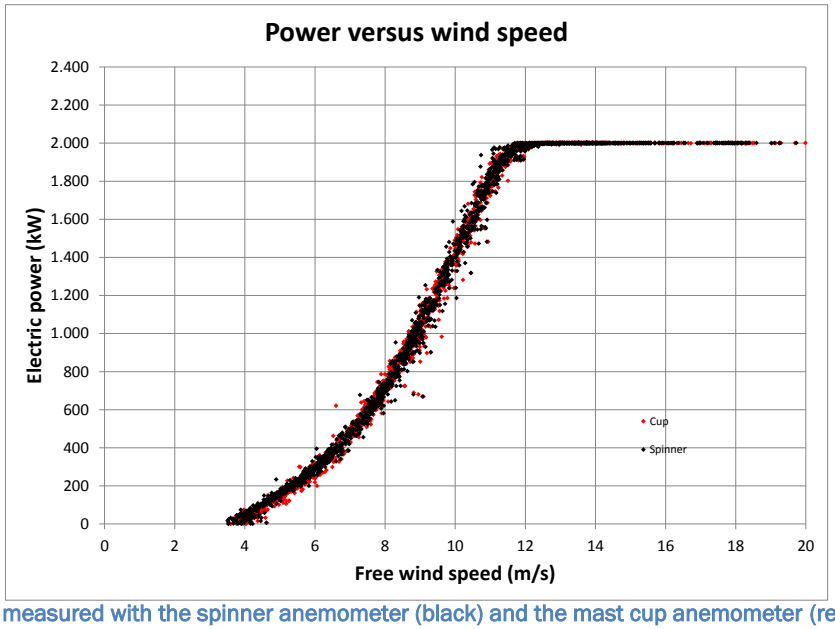

Figure 5.7 Power curves measured with the spinner anemometer (black) and the mast cup anemometer (red) where induction is corrected for with the induction function

5.8 Overview of calibrations relevant to measurement and control

The following table gives an overview of calibrations that are relevant to different types of measurements.

Table 1 Table of calibrations relevant to different types of measurements with spinner anemometers

	Zero wind calibration	Wind tunnel calibration	Internal SA calibration	Inflow angle calibration	Wind speed calibration	NTF calibration IEC61400-12-2
Yas misalignment	X		X	X*		
Inflow angle measurements	X		X	X*		
Wind speed measurements	X		X	X*	X’	
Free wind speed measurements with NTF	X		X	X*	X’	X’
Turbulence measurements	X		X	X*	X’	X’
Shear measurements	X		X	X*	X’	X’
Environmental measurements	X		X	X*	X’	X’
Relative power curve measurements	X		X	X*	X’	
Power curve measurements IEC61400-12-2	X	X	X	X*	X’	X’
Loads measurements IEC61400-13	X	X	X	X*	X’	X’

* Calibration is needed for the type of wind turbine with specific spinner and blade root design

6.0 Cost Benefit Analysis of LIDAR and Spinner Anemometer based Measurements

Where LIDAR is used to reduce fatigue loads, it is relatively straightforward to assess the implications. Only the average rate of fatigue damage accumulation over the lifetime is important. Even if the LIDAR is unavailable for some fraction of the time, for whatever reason, this can be taken into account.

It is tempting to think that if fatigue loads are being reduced, there should also be a reduction in extreme operational loads caused by turbulence (as opposed to extreme loads caused by malfunctions, grid loss, non-operational conditions, etc.). However, even if this is true and the extreme loads happen to be design-driving, it may be difficult to take advantage of this in reducing the design load envelope, for a number of reasons as discussed for example in[16]. One problem is the need to understand the probability of availability of a good LIDAR signal at the moment when the extreme load happens – even if the probability of unsuitable atmospheric conditions is low, one would have to be sure that such conditions are not highly correlated with the very conditions which might give rise to that extreme wind event.

A bigger problem is how to define that extreme wind event itself: current extreme gusts are specified only in terms of changes in speed, direction and shear parameters at the turbine rotor, but if LIDAR preview is used to mitigate the effect of the gust one would also have to specify the spatial structure of the gust and how it moves during the LIDAR look-ahead time. Current gust specifications are already very arbitrary and physically unrealistic, and to extend the specification to include these effects is to stretch credibility still further. One possibility currently being investigated is to generate simulated turbulent wind fields with embedded gusts; but even these models are likely to use Gaussian assumptions which are most likely to break down in extreme conditions, and may in any case be quite unrepresentative of the conditions which actually cause the most extreme loads. For example, an extreme coherent gust as currently used could represent the arrival of something like a thunderstorm front, and if this front sweeps in from the side and a forward-facing LIDAR fails to detect it, the loading might actually be more severe than if LIDAR-based control was not used: the LIDAR-based control typically achieves its main benefit by using lower pitch control feedback gains, which would result in much higher over-speeding when the undetected gust arrives, resulting in higher peak loads, and perhaps causing a shutdown which would otherwise have been avoided.

The Spinner Anemometer on the other hand has been much lesser used in wind turbine control, but it has great potential based on the accuracy of measuring the wind conditions. The spinner anemometer can in-principle be integrated into the wind turbine control system even without significantly altering the control algorithms. For example, the accuracy in yaw measurements as shown in the previous chapter, allows ease of yaw detection within a narrow range which can reduce the fatigue damage equivalent loads. The DLC 1.2 load case that is simulated to quantify fatigue damage in wind turbines usually uses a yaw misalignment of the order of 10 degrees. With the spinner anemometer installed, the

same load case may be run without yaw misalignment or with a minor misalignment of 5 degrees, which can result in fatigue damage reduction.

The effectiveness is measuring turbulence can also be used to better quantify the loads being borne by the turbine components and this can allow effective condition monitoring and remaining life prediction of components. The increase in power capture from lower yaw misalignments and better knowledge of turbulence leading to lower uncertainties in power prediction can translate to lower LCOE.

From INNWIND deliverable report D1.22, it is seen that increasing the capacity factor from 0.40 to 0.45 leads to a reduction in LCOE by 10 €/MWh which is equivalent to the reduction resulting from cutting the CAPEX down by 500 €/kW. Therefore if a LIDAR or spinner anemometer can increase capacity factors while mitigating loads, the benefits can easily outweigh the costs accrued in the instrumentation and added control algorithms.

References

[1] D. Schlipf and M. Kühn, "Prospects of a collective pitch control by means of predictive disturbance compensation assisted by wind speed measurements," in Proceedings of the German Wind Energy Conference DEWEK, Bremen, Germany, 2008.

[2] D. Schlipf, T. Fischer, C. E. Carcangiu, M. Rossetti, and E. Bossanyi, "Load analysis of look-ahead collective pitch control using LiDAR," in Proceedings of the German Wind Energy Conference DEWEK, Bremen, Germany, 2010.

[3] E. Bossanyi, "Un-freezing the turbulence: improved wind field modelling for investigating lidar-assisted wind turbine control," in Proceedings of the European Wind Energy Association annual event, Copenhagen, Denmark, 2012.

[4] E. Simley and L. Y. Pao, "A longitudinal spatial coherence model for wind evolution based on large-eddy simulation," in American Control Conference (ACC), 2015, Chicago, Illinois, USA, July 2015, pp. 3708–3714.

[5] D. Schlipf, F. Haizmann, N. Cosack, T. Siebers, P.W. Cheng,"Detection of Wind Evolution and Lidar Trajectory Optimization for Lidar-AssistedWind Turbine Control," Meteorologische Zeitschrift, PrePub DOI 10.1127/metz/2015/0634.

[6] A. Scholbrock, P. Fleming, L. Fingersh, A. Wright, D. Schlipf, F. Haizmann, and F. Belen, "Field testing LIDAR based feed-forward controls on the NREL controls advanced research turbine," in Proceedings of the 51st AIAA Aerospace Sciences Meeting Including the New Horizons Forum and Aerospace Exposition, Dallas, USA, 2013.

[7] D. Schlipf, P. Fleming, F. Haizmann, A. Scholbrock, M. Hofsäß, A. Wright, and P. W. Cheng, "Field testing of feedforward collective pitch control on the CART2 using a nacelle-based lidar scanner," Journal of Physics: Conference Series, vol. 555, no. 1, p. 012090, 2014.

[8] F. Haizmann, D. Schlipf, S. Raach, A. Scholbrock, A. Wright, C. Slinger, J. Medley, M. Harris, E. Bossanyi, and P. W. Cheng, "Optimization of a feed-forward controller using a cw-lidar system on the CART3," in American Control Conference (ACC), 2015, Chicago, Illinois, USA, July 2015, pp. 3715–3720.

[9] F. Haizmann, D. Schlipf, N. Cosack, D. Neuhaus, S. Raach, T. Maul, P. W. Cheng, "Field testing of lidar assisted feed-forward control on a large commercial wind turbine," Poster at the European Wind Energy Association Annual Event (EWEA), Barcelona, Spain, 2014.

[10] E. Simley and L. Y. Pao, "Correlation between rotating LIDAR measurements and blade effective wind speed," in Proceedings of the 51st AIAA Aerospace Sciences Meeting Including the New Horizons Forum and Aerospace Exposition, Dallas, USA, 2013.

[11] D. Schlipf, J. Mann, and P. W. Cheng, "Model of the correlation between lidar systems and wind turbines for lidar assisted control," Journal of Atmospheric and Oceanic Technology, vol. 30, no. 10, pp. 2233–2240, 2013.

[12] E. Simley and L. Y. Pao, "Reducing lidar wind speed measurement error with optimal filtering," in Proceedings of the American Control Conference, Washington, USA, 2013.
[13] F. Dunne and L. Y. Pao, "Benefit of wind turbine preview control as a function of measurement coherence and preview time," in Proceedings of the American Control Conference, Washington, USA, 2013.
[14] G. I. Taylor, "The spectrum of turbulence," Proceedings of the Royal Society of London. Series A - Mathematical and Physical Sciences, vol. 164, no. 919, pp. 476–490, 1938.
[15] F. Dunne, L. Y. Pao, D. Schlipf, and A. K. Scholbrock, "Importance of lidar measurement timing accuracy for wind turbine control," in Proceedings of the American Control Conference, June 2014, pp. 3716–3721.
[16] E. Bossanyi, A. Kumar, and O. Hugues-Salas, "Wind turbine control applications of turbine-mounted lidar," Journal of Physics: Conference Series, vol. 555, no. 1, p. 012011, 2014.
[17] I. Elorza, M. Iribas, and E. Miranda, "On the feasibility and limits of extreme load reduction for wind turbines via advanced sensing: A lidar case study," in Proceedings of the American Control Conference, Washington, USA, 2013.
[18] F. Dunne, L. Y. Pao, A. D. Wright, B. Jonkman, and N. Kelley, "Combining standard feedback controllers with feedforward blade pitch control for load mitigation in wind turbines," in Proceedings of the 48th AIAA Aerospace Sciences Meeting Including the New Horizons Forum and Aerospace Exposition, Orlando, USA, 2010.
[19] N. Wang, "Lidar-assisted feedforward and feedback control design for wind turbine tower load mitigation and power capture enhancement," Ph.D. dissertation, Colorado School of Mines, 2013.
[20] M. Harris, M. Hand, and A. Writght, "Lidar for turbine control," NREL, Tech. Rep. TP-500-39154, January 2006.
[21] J. Laks, L. Y. Pao, A. Wright, N. Kelley, and B. Jonkman, "Blade pitch control with preview wind measurements," in Proc. AIAA Aerospace Sciences Meeting, Orlando, Florida, USA, January 2010.
[22] F. Dunne, D. Schlipf, L. Y. Pao, A. D. Wright, B. Jonkman, N. Kelley, and E. Simley, "Comparison of two independent lidar-based pitch control designs," in Proc. AIAA Aerospace Sciences Meeting, Nashville, Tennessee, USA, January 2012.
[23] Pedersen TF, Madsen HA, Møller R, Courtney, M, Sørensen NN, Enevoldsen P, Egedal P, "Spinner Anemometry – An Innovative Wind Measurement Concept", EWEC2007 Milan, paper and poster
[24] T. Mikkelsen, N. Angelou, K. Hansen, M. Sjöholm, M. Harris, C. Slinger, P. Hadley, R. Scullion, G. Ellis, and G. Vives. A spinner-integrated wind lidar for enhanced wind turbine control. *Wind Energy*, 16(4):625–643, 2013.
[25] C. Hill. D6.14.1 Remote Sensing (UpWind WP6) QinetiQ Lidar Availability Re- port. Technical report, The UpWind project, 2010.
[26] A. Woodward at Zephirlidar. Personal communication. July 2015.
[27] Pedersen TF, Sørensen NN, Vita L, Enevoldsen P, Optimization of Wind Turbine Operation by Use of Spinner Anemometer, Risø-R-1654(EN), August 2008

[28] Pedersen TF, Demurtas G, Zahle F, “Calibration of a spinner anemometer for yaw misalignment measurements”, Wind Energy 2014, we1798
[29] Pedersen TF, Demurtas G, Gottschal J, Højstrup J, Nielsen JD, Christiansen W, Weich G, Sommer A, Kristoffersen JR, Improvement of Wind Farm Performance by Means of Spinner Anemometry, DTU Wind Energy E-0040, December 2013
[30] Pedersen TF, Demurtas G, Sommer A, Højstrup J, Measurement of rotor centre flow direction and turbulence in wind farm environment, Journal of Physics: Conference Series (Online), Vol. 524, No.1, 012167, 2014
[31] Højstrup J, Nielsen D, Hansen K, Lauritzen L, Maximise energy production by minimizing yaw misalignment. Large scale field deployment of spinner anemometer. Poster 0162, EWEC 2013, Vienna, 2013, Poster award
[32] CBC 0C Decision/Clarification Sheet, Subject: Use of Spinner Anemometers, IEC61400-12-2: 2013, Annex H, 2012-02-02, CAC/CBC, draft
[33] IEC 61400-12-1, Wind turbines – part 12-1: Power performance measurements of electricity producing wind turbines, 2005, International Electrotechnical Commission
[34] IEC 61400-12-2, Wind turbines – part 12-2: Power performance measurements of electricity producing wind turbines based on nacelle anemometry, 2013-03, International Electrotechnical Commission
[35] ASTM D 6011 – 96 (reapproved 2003), Standard Test Method for Determining the Performance of a Sonic Anemometer/Thermometer, 2003
[36] Demurtas G, Pedersen TF, Zahle, Calibration of a spinner anemometer for wind speed measurements, Wind Energy (submitted 2015)
[37] Demurtas G, Power curve measurement with spinner anemometer according to IEC 61400-12-2, September 2015
[38] Højstrup J, Power curve measurements using the ROMO Wind Spinner Anemometer, May 2013, www.pcwg.org
[39] IEC 61400-12-13, Wind turbines – Part 13: Measurement of mechanical loads, 88/511/CDV, 2015, International Electrotechnical Commission
[40] Hansen JK, Højstrup J, Method for controlling the pitch angle of at least one wind turbine blade, Patent application US2015/0139796 A1, May 21, 2015


INNWIND
EU